

Ambipolar Property of Isolated Hydrogen in Oxide Materials Revealed by Muon

M. Hiraishi,¹ H. Okabe,¹ A. Koda,^{1,2} R. Kadono,^{1,2,3,*} and H. Hosono³

¹*Muon Science Laboratory and Condensed Matter Research Center, Institute of Materials Structure Science, High Energy Accelerator Research Organization (KEK-IMSS), Tsukuba, Ibaraki 305-0801, Japan*

²*Department of Materials Structure Science, The Graduate University for Advanced Studies (Sokendai), Tsukuba, Ibaraki 305-0801, Japan*

³*Materials Research Center for Element Strategy, Tokyo Institute of Technology (MCES), Yokohama, Kanagawa 226-8503, Japan*

(Dated: September 16, 2022)

The study on the electronic state of muon as pseudo-hydrogen (represented by the elemental symbol Mu) by muon spin rotation has long been appreciated as one of the few methods to experimentally access the electronic state of dilute hydrogen (H) in semiconductors and dielectrics. Meanwhile, theoretical predictions on the electronic state of H in these materials by first-principles calculations using density functional theory (DFT) do not always agree with the observed states of Mu. In order to address this long-standing issue, we have re-examined the vast results of previous Mu studies in insulating/semiconducting oxides with special attention to the non-equilibrium character and the ambipolarity of Mu. As a result, we established a semi-quantitative model that enables systematic understanding of the electronic states of Mu in most oxides. First of all, Mu often occurs simultaneously in a neutral (Mu^0) and a diamagnetic state (Mu^+ or Mu^-) in wide-gap oxides. This is not explained by DFT calculations, as they predict that H is stable only in a diamagnetic state with the polarity determined by the equilibrium charge-transition level ($E^{+/-}$). Our model considers that μ^+ interacts with self-induced excitons upon implantation to form relaxed-excited states corresponding to a donor-like (Mu_D) and/or an acceptor-like (Mu_A) states. Moreover, these states are presumed to accompany the electronic level ($E^{+/0}$ or $E^{-/0}$) predicted by the DFT calculations for H. By considering that the stability of these two states including their valence is determined by i) the relative position of $E^{\pm/0}$ in the energy band structure of the host and ii) a potential barrier associated with the transition between Mu_D and Mu_A , we find that the known experimental results can be explained systematically in accordance with $E^{\pm/0}$. The model also reveals some common properties of Mu-related defects which were previously regarded as individual anomalies. One is the polaron-like nature of the electronic states associated with shallow donor Mu complexes, for which we argue a major shift of the viewpoint to the Mu_D^+ -bound excitons. Another is the fast diffusion of Mu_A^0 , which is understood by the isolated feature of the acceptor-like electronic states. The possible impacts of these findings to a wide range of insulating compounds is discussed by drawing on examples such as GaN, FeS_2 , and NaAlH_4 as key materials for the green technologies.

I. INTRODUCTION

Hydrogen (H) is conventionally categorized as one of the group 1 elements on the periodic table. This is because H, like alkali metals, readily donates electrons in many redox reactions. On the other hand, it is also well known that H takes a relatively stable anion (hydride) state. In this case, H can be regarded as an element in the same family as halogens (group 17). Since it became known in the 1980s that H can interact with both *n*-type and *p*-type impurities in silicon and greatly affect the electrical conductivity [1, 2], H has been attracting considerable attention as a special impurity that exhibits ambipolarity in the field of semiconductors.

It is known from previous studies that most of the incorporated H forms complexes with other impurities and defect centers such as atomic vacancies, thereby causing passivation (loss of electrical activity). Unlike the transfer of electrons between impurity levels (carrier compensation) that occurs when both *n*-type and *p*-type defect centers coexist, the impurity levels themselves are eliminated from the band gap in the passivation due to solid-state chemical reactions. Such complex defects have already been analyzed by various experimental techniques, and their local structures are being clarified.

Meanwhile, another important issue is the electrical activity of H itself as a defect center. It is expected that a few ppm of H (equivalent to about $\sim 10^{15}$ – $10^{16}/\text{cm}^3$) can be easily incorporated into the material unintentionally during the manufacturing process. This is comparable to the carrier concentration caused by deliberate impurity addition, thus having a significant impact on conductivity by itself. Including this point, understanding the local electronic state of isolated H is of fundamental importance in elucidating the entire mechanism of contribution for H to electrical activity in semiconductors at the atomic level. However, the amount of isolated H in bulk solids is relatively small, and spectroscopic techniques to investigate its local electronic state are limited.

The muon spin rotation (μSR) is one of such techniques to obtain the relevant information by implanting a positively charged muon (μ^+ , hereafter simply called muon) into the target material and investigating its electronic state as pseudo-H. The muon is an unstable subatomic particle, and it is available as a particle beam in dedicated accelerator facilities. It behaves as a light radioactive isotope of the proton (with about 1/9 of the proton mass) in terms of chemical properties upon incorporation into matter. This is because the muon mass is two orders of magnitude larger (about 206 times) than the electron mass, and thus making the adiabatic approximation sufficient for understanding muon-electron interaction. As a matter of fact, the difference in the Bohr radius between a muon binding a single electron, called muonium, and the cor-

* ryosuke.kadono@kek.jp

responding neutral H atom is only 0.43%, so that they can be regarded as having practically the same electronic structure.

On the other hand, the light mass of muon compared with H assumes relatively large isotope effects on the dynamical properties such as diffusion in solids. For example, the zero-point energy E_0 is proportional to the square root of the particle mass in a harmonic potential. Since muon/muonium has nearly 3 times greater E_0 than that of H, the activation energy for the former in the over-barrier hopping motion is reduced by $\sim 2E_0$. The large zero-point motion also leads to a greater tunneling probability to the neighboring sites, thus enhancing tunneling-mediated diffusion (quantum diffusion). While the present work is mostly concerned with the quasistatic local electronic properties, we will refer to the quantum diffusion of muonium at low temperatures in Sect. IV D as an example for the quantum diffusion.

In the discussion on muon as pseudo-H, it is convenient to have the elemental name. Hereafter, the symbol Mu will be used for this purpose (corresponding to H for hydrogen), and the valence states of Mu will be denoted as Mu^+ , Mu^0 , and Mu^- .

Since the dawn of μSR research in 1970s, various electronic states and dynamics of Mu have been experimentally revealed in a wide variety of materials including oxides. In addition, the recent progress of first-principles calculations using density functional theory (DFT) in accordance with the advent of computational environment has made it possible to discuss the local electronic structures of Mu/H in individual materials in great detail. Meanwhile, the construction of a physical model that would allow us to understand the Mu states in a cross-material way is still in its infancy. Related with this, relatively little attention has been paid to the ambipolarity of Mu/H in itself, and the mainstream of research to date has been concerned with the donor-like behavior of Mu/H as a member of group I elements.

In this paper, we will show that the ambipolar property of Mu/H, including its acceptor-like behavior, is the key to the coherent understanding of the local electronic state of Mu. We also argue that the fact that we experimentally observe such ambipolar Mu states is inextricably linked to the another fact that the initial state of Mu is in a temporary non-thermal equilibrium state. The primary goal of this paper is to construct a semi-quantitative model for a unified understanding of the electronic structure of Mu by properly taking into account these two factors.

To this end, we have compared the experimentally observed electronic states of Mu in various oxides with those predicted by DFT calculations for H in the respective oxides published to date; it is not the scope of this paper to examine the precision of previous calculations by performing new ones by ourselves. In fact, the results of these existing calculations constitute the basis for our model, and it could be argued that the success of the model serves as evidence that they are sufficiently reliable for our goal. While we provide a brief summary on the general aspects of the DFT calculations in Sect. III A, readers are encouraged to refer to the individual references cited in Table I in Sect. IV B for their details.

II. NOTABLE FEATURES OF μSR AS A METHOD FOR STUDYING PSEUDO-HYDROGEN

In the actual μSR experiment, nearly 100% spin-polarized μ^+ is implanted into a sample, and the time-dependent spatial asymmetry ($\simeq 20\%$) of positrons emitted with high probability in the direction of spin polarization upon beta decay is observed. When μ^+ is implanted into a solid material, it decelerates in a short time (generally less than 1 ns) and comes to rest at an interstitial position. From that moment until the beta decay occurs (with the mean lifetime $\tau_\mu = 2.198 \mu\text{s}$), μ^+ behaves as Mu to take a variety of valence states according to the local environment. The muon spin exhibits precession at a frequency proportional to the hyperfine interaction between Mu and the surrounding electrons and/or nuclear spins. The hyperfine interaction is described by the Hamiltonian

$$\mathcal{H}/\hbar = \gamma_\mu \mathbf{H}(\mathbf{r}) \cdot \mathbf{S}_\mu = \frac{1}{2} [2\pi \mathbf{A}(\mathbf{r})] \cdot \mathbf{S}_\mu, \quad (1)$$

where γ_μ is the muon gyromagnetic ratio ($= 2\pi \times 135.53 \text{ MHz/T}$), \mathbf{S}_μ is the muon spin operator, and $\mathbf{H}(\mathbf{r})$ is the effective hyperfine field [$\mathbf{A}(\mathbf{r})$ being the hyperfine parameter] at the Mu position \mathbf{r} in the crystalline lattice [3]. Because of the large difference in $\mathbf{H}(\mathbf{r})$, the paramagnetic state (Mu^0) can be readily discerned from the diamagnetic state (Mu^+ or Mu^-) by the μSR frequency spectrum (see Appendices A and B for more details). In contrast, the distinction between Mu^+ and Mu^- needs high-precision chemical shift measurements ($\sim 10^1$ ppm) [4]. The time evolution of the muon polarization is observed as a statistical average of the signals from a large number of Mu over a time period of about $10\tau_\mu$ ($\sim 20 \mu\text{s}$), with $t = 0$ defined by the time of μ^+ arrival.

Here, we would like to mention some practically important features for Mu in mimicking H. First, the penetrating power of the muon beam is sufficiently large so that it should not be affected by the surface condition of the sample (bulk-sensitive). The effective concentration of the implanted muons is extremely dilute; even in a pulsed beam experiment where a large number of muons are injected at once, the number of muons present in the sample at the same time is at most $\sim 10^4/\text{cm}^2$ per cross section. The stopping range for muons with a typical incident energy of $T_\mu \simeq 4 \text{ MeV}$ is about 0.1–1 mm from the sample surface, so their volume concentration is less than $\sim 10^5$ muons per cm^3 . Moreover, it does not accumulate in the sample, as it disappears in a short time ($\sim \tau_\mu$). Therefore, muons provide a unique opportunity to observe the electronic state of pseudo-H in the true dilute limit.

Meanwhile, as will be explained in detail in Sect. III, the initial state of the implanted Mu is mostly in a relaxed-excited (metastable) state caused by the interaction with the electron-hole pairs (or excitons) generated by the transfer of T_μ along the muon track to the host lattice. This is also implied by experiments with recently available low-energy muon beam (LEM, $T_\mu \simeq 1\text{--}30 \text{ keV}$ at Paul Scherrer Institute, Switzerland), in which muons are implanted into a region of $10^1\text{--}10^2$ nanometers from the sample surface. Although the Mu density in this case is still in the dilute limit, it has been demonstrated that the fractional yields of Mu in different valence

states are strongly dependent on T_μ [5], indicating the definitive influence of Mu-exciton interaction in determining the final Mu states.

That the electronic state of Mu does not necessarily correspond to the thermal equilibrium state of H may seem to imply its limitations as a source of information for H. However, as discussed below, it is this non-equilibrium nature that allows us to use Mu to experimentally evaluate the ambipolarity of H. In addition, it should be noted that many electronic materials, including oxides, are used in devices under various electronic excitations such as electric fields and optical irradiation. In this regard, the information obtained from Mu will provide microscopic clues for clarifying the effect of H in those materials on their performance under such electronic excitations (see Sect. IV C, for example). Thus, Mu serves as a complementary tool to H itself to reveal the whole picture on the behavior of H in matter.

III. MU STUDY—AN APPROACH FROM NON-THERMAL EQUILIBRIUM STATES

A. DFT calculations for H defect centers

In general, the formation energy E^q of H defect centers as a function of the Fermi level E_F is estimated by DFT calculations using the following equation,

$$E^q(E_F) = E_t[\text{H}^q] - E_t[-] + qE_F - n_H\mu_H \quad (2)$$

where $E_t[\text{H}^q]$ and $E_t[-]$ denote the total energy of a supercell involving H^q and a perfect cell, respectively, calculated for charge q ($= \pm, 0$), n_H is the number of H atoms, and μ_H is the reference chemical potential for H [6]. Provided that

$$E_t[\text{Mu}^q] = E_t[\text{H}^q],$$

which is valid within the adiabatic approximation, Eq. (2) gives the formation energy for Mu^q as schematically shown in Fig. 1a. Although Mu/H can play the role of either a cation or an anion with respect to the host, their local structures can be different with each other (Fig. 1b). Therefore, we refer to them as Site-*D* (donor-like, associated with anions) and Site-*A* (acceptor-like, associated with cations). In addition, among the three charge-transition energies, the equilibrium charge-transition level ($E^{+/-}$) is lower than the acceptor/donor level ($E^{\pm/0}$) in most cases (see Fig. 1a). This behavior is characteristic for systems with strong electron-phonon coupling [7], indicating that the effective onsite Coulomb repulsion energy (U) is negative. The negative U character combined with the ambipolarity leads to a tendency of charge disproportionation for H (i.e., preferring H^\pm to H^0 states) [8, 9]. The electronic state of H in the thermal equilibrium is then determined by the relationship among $E^+(E_F)$, $E^0(E_F)$, and $E^-(E_F)$. More specifically, only H_D^+ ($E_F < E^{+/-}$) or H_A^- ($E_F > E^{+/-}$) will be realized, and thus $E^{+/-}$ will be the effective impurity level.

In order to predict the electrical activity of H defects by DFT calculations, it is necessary to be able to predict the band

structure of the defect-free host with the accuracy comparable with that for $E^q(E_F)$. However, early DFT calculations exhibited common tendencies that i) they significantly underestimate the band gap, and that ii) the charged defect levels are sensitive to corrections for the finite supercell size, and various correction methods have been developed to mitigate these problems [10]. Most of the DFT calculations we referred to for oxides were done in the last decade, and they are expected to reflect the results of such developments. Meanwhile, it is also expected that the results of these calculations may be skewed to some extent by differences in the actual prescriptions adopted for the correction.

In this regard, it is noteworthy that, among the 18 oxides in Table I on which our model is based, 9 of them rely on the single set of calculations performed by Li and Robertson [11]. This may be helpful in assessing the systematic reliability of the DFT calculations. According to Ref. [11], their calculations were carried out using the plane wave pseudopotential code CASTEP [12]. More specifically, norm-conserving pseudopotentials were used to represent the atomic potentials. The cutoff energy for plane waves was 800 eV. For the hybrid functional, the one introduced by Heyd-Scuseria-Ernzerhof (HSE06) was employed [13, 14]. To correct the band gap errors of pure Generalized Gradient Approximation (GGA), a fraction α of the short-range separated part of the Hartree-Fock (HF) exchange was combined with the GGA exchange-correlation integral, where α was varied to fit the band gap for systems with a greater gap. The screening length was set to $\mu = 0.106$ bohrs⁻¹ [14]. The calculated band gap energies are quoted in Table I for comparison with experimental values.

For the defect calculations in Ref.[11], the lattice parameters for crystalline oxides were set to experimental values, and only the internal atomic coordinates for the interstitial H were relaxed. The electronic states turned out to be localized enough to save supercell size; they needed supercells with 33-49 atoms each for diverse oxides. The H atom was positioned in an arbitrary location near the open interstitial site's center. The cutoff energy was 800 eV, and the k point mesh was $2 \times 2 \times 2$. The defect formation energies were calculated by Eq. (2), where the reference chemical potential was defined by following the method described in Ref. [10].

B. Mu as relaxed-excited states and acceptor/donor levels

The attempt to interpret the electronic states of Mu in terms of $E^{+/-}$ fails to explain the existence of the paramagnetic Mu^0 state reported in many wide-gap oxides (see Table I). This necessitates the introduction of the hypothesis that the initial Mu state immediately after μ^+ implantation to rest corresponds to a relaxed-excited state upon rapid quenching from infinite temperature [i.e., $\beta \equiv 1/k_B T \rightarrow 0$ in the partition function $Z(\beta)$; see Appnd. C]. The relative yields of the final states are determined by the density of states for the available sites and valence states around a common formation energy irrespective of E_F .

Here, an intriguing fact to remember for considering the origin of Mu^0 is that interstitial paramagnetic H centers (H_i^0)

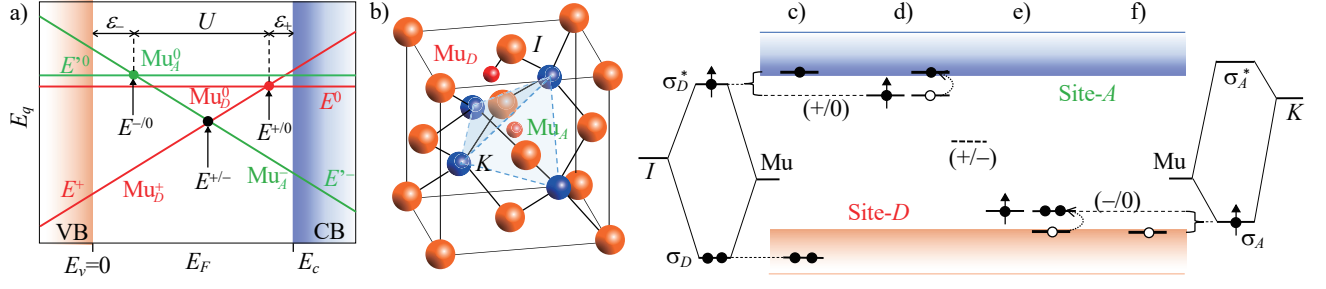
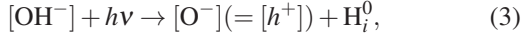


FIG. 1. a) Schematic illustrations for the formation energy (E^q) of Mu^q ($q = 0, \pm$) vs Fermi energy (E_F), b) the local structure of a donor-like center (Mu_D at Site-D, bonded to an I anion) and an acceptor-like center (Mu_A at Site-A, bonded to K cations) in binary compounds, c)–f) the corresponding band diagrams derived from molecular orbital models (where arrows indicate spin-degrees of freedom for localized electrons); $(+/-)$ refers to the equilibrium charge-transition level, $(+/0)$ to the donor level (c,d), and $(-/0)$ to the acceptor level (e,f).

are produced by irradiation of H-containing ionic crystals with ultraviolet (uv) light at low temperatures. For example, it is known that H_i^0 (known as U_2 -centers) is produced in alkali halides containing OH^- defects in the photodissociation reaction,

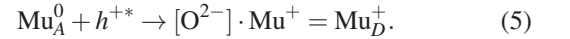
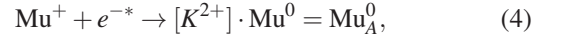


where $[\]$ refers to the anion substitutional site, $h\nu$ to the photons, and h^+ to the hole [15–17]. This is considered to be a process similar to that of self-trapped-exciton (STE) formation by electronic excitation of the halogen sublattice, $2\text{X}^- + h\nu \rightarrow [\text{X}_2^-] (= [h^+]) + e_i^-$, with X denoting the halogen atoms. (It is known that holes comprise X_2^- dimers in alkali halides [18].) Since excited electrons are not self-trapped by themselves [19], the STE formation is understood as the capture (localization) of excited electrons by the Coulomb interaction with self-trapped holes. Thus, it is interpreted that $[\text{O}^-]$ corresponds to the self-trapped h^+ , and H_i^0 to e^- captured by H_i^+ (in place of h^+), respectively. The H_i^0 state in alkali halides is presumed to be stabilized by the antibonding character with halogen atoms [20] and the bonding character with alkali metals: it must be noted that the excited electron is a dangling bond for the cation. It is well known that the atomic Mu^0 state observed in alkali halides can be regarded as the counterparts of the H_i^0 center [21], where the electronic excitation is induced by the kinetic energy of incident muon; it is estimated that $\sim 10^3 e^-h^+$ pairs (excitons) are produced from 4 MeV muons [19]. Regarding oxides, a process similar to Eq.(3) has been reported in OH-containing α - SiO_2 (silica) upon the exposure to ionizing radiations at low temperatures [22–27]. Here, it is reasonable to assume that the excited electrons on Si $3p$ orbitals [28, 29] are eventually captured by H_i^+ (that mimics the role of h^+ localized on O).

These observations strongly suggest that H_i^0 centers (and corresponding Mu_A^0 states) exist as the relaxed-excited state, accommodating the electron in the acceptor level. In other words, the H_i^+ (Mu_A^+) state created immediately after the electronic excitation serves as a center of complex formation analogous to the “acceptor-bound exciton” [30]. Evidence for the interaction between Mu^+ and excitons (not just electrons) is found, for example, in the blueshift (~ 0.5 eV) of the luminescence from muon-induced STE’s in KBr [31, 32]. This

blueshift can be now attributed to the formation of the ionized Mu^0 -bound exciton, where the luminescence occurs between h^+ and e^- bound to Mu^0 upon the annihilation of μ^+ by the beta decay, $[\text{X}_2^-] \cdot \text{Mu}^0 \rightarrow [\text{X}_2^-] \cdot e_i^- \rightarrow 2\text{X}^- + h\nu$, where the lattice relaxation for e^- is presumed to be smaller than that for the native STE.

Considering that Mu in oxides acts as a trapping center for the self-induced free excitons, the initial electronic state of the ambipolar Mu is not limited to the acceptor-like state. For example, let us examine mono-oxides, KO (with K denoting the divalent cations). The free exciton electrons and holes, conveniently expressed as e^{-*} , h^{+*} , interact with Mu to form the states respectively corresponding to the Mu_A and Mu_D states, i.e.,



It is known that the yield of Mu_A^0 is actually bottlenecked by the electron supply from ionization trails [5, 33–35]. While both electrons and holes are not self-trapped in many oxides including Al_2O_3 , MgO , ZnO , and crystalline SiO_2 , holes are self-trapped in α - SiO_2 and in alkali halides [19]. In the latter case, the yield of Mu_D^+ may depend on the mobility of Mu_A^0 (see Sect. IV D).

Mu_D^+ is likely to have a good chance of capturing another electron to become Mu_D^0 (which may be equivalent with “donor-bound excitons”). In fact, there are known examples of donor-like H/Mu defect centers in ionic compounds including oxides. One such classical example in the alkali halides is the hydrogen bifluoride complex, $\text{F}^- \cdot \text{H}^+ \cdot \text{F}^-$. This is also known as a prototype of strong hydrogen bonding observed upon X-ray irradiation [36]. The analogous $\text{F}^- \cdot \text{Mu}^+ \cdot \text{F}^-$ complexes have been reported in various alkali fluorides and alkaline earth fluorides. They are readily identified by the characteristic μSR signal due to a well-defined magnetic dipolar field exerted from the two ^{19}F nuclei (spin $I = 1/2$) [37]. The donor-like character is evident in the presumed formation process, $\text{Mu}^0 + h^{+*} (= \text{F}_2^-) \rightarrow \text{F}^- \cdot \text{Mu}^+ \cdot \text{F}^-$. Note that these donor-like states often coexist with Mu_A^0 [21]. The occurrence of two different paramagnetic centers corresponding to Mu_D^0 and Mu_A^0 are well established in elemental (group 4) and group

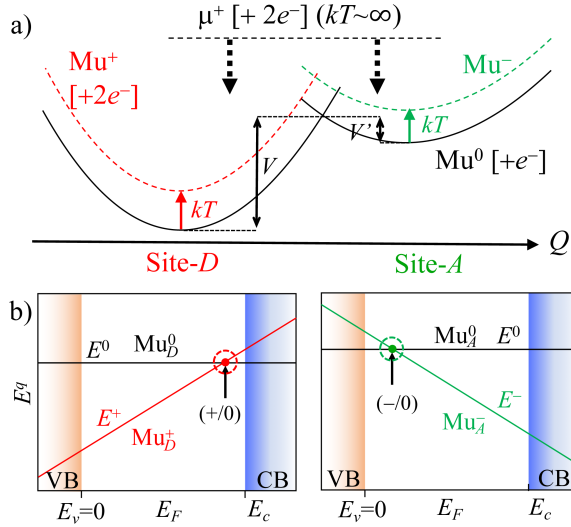


FIG. 2. a) Adiabatic potential curves for Mu in binary compounds, where each curve represents Sites-D and -A with different valences. (NB: those for Mu^\pm depends on E_F .) If there is a potential barrier between Site-D and -A (e.g., V and V' between Mu^0 states), both are observed simultaneously (Q is the configuration coordinate). b), c) The electronic states of Mu relevant to the respective sites are shown by dashed circles in the E^q vs E_F diagram.

13-15 compound semiconductors [1, 38].

This renewed “radiolysis model” with emphasis on the Mu-exciton interaction not only provides a microscopic model of Mu^0 formation but also retain the merit of explaining the finite yield of Mu^0 by electron-supply-limited processes. But the model fails to account for the increase in the initial Mu^0 yield with increasing temperature in place of the diamagnetic state, e.g., in Lu_2O_3 [39]. This has led to the introduction of the “thermal spike” model [40]. In this model, the effective local lattice temperature is presumed to be temporally elevated by phonon excitation (within the time scale of sub-picoseconds) around the Mu stopping position. The thermal spike model has a long history of its own since 1960s [41], developed to understand the localized damage around ion tracks during irradiation of materials by heavy ions and fission products. The model for the initial Mu states is concerned with the kinetic energy range lower than that leading to atomic displacements by the knock-on processes.

Considering the above discussions, we assume that the initial state of Mu is determined roughly through two steps. First, immediately after coming to rest, Mu forms ambipolar relaxed-excited states represented by an adiabatic potential shown in Fig. 2a [19]. The critical hypothesis here is that these states correspond to Mu_A^0 and/or Mu_D^0 in Fig. 1a originally predicted for H by the *ab initio* DFT calculations. The situation can be described as that attained by the temporary shift of E_F from thermal equilibrium to the region $E^\pm(E_F) > E^0(E_F)$. The variation of these states with temperature is then interpreted to reflect the degree of relaxation for E_F from around $E^{\pm/0}$ towards $E^{+/-}$ within the observation time ($< 10^{-5}$ s) at each temperature. For instance, regarding Mu_D in Fig. 2b, the transition from Mu_D^0 to Mu_D^+ occurs

as the temporal E_F decreases from the middle between $E^{+/0}$ and E_c to the equilibrium level (either $E^{+/-}$ of Mu/H or other impurities, leaving the $E^{+/0}$ level empty) with increasing temperature ($k_B T \gg \varepsilon_+$), which is interpreted as the promotion of an electron from the $E^{+/0}$ level to the conduction band (see Fig. 1d). Therefore, if $E^{+/0}$ is located within the band gap, Mu_D^0 can be realized as the initial state. Meanwhile, if $E^{+/0}$ is in the conduction band ($E^{+/0} > E_c$) and there is no barrier associated with charge conversion, Mu_D^0 will immediately ionize and take the Mu_D^+ state (Fig. 1c), meaning that it behaves as an *n*-type impurity regardless of temperature. The same is true for the *p*-type activity of Site-A (Figs. 2c, 1e and 1f).

Moreover, if the Mu_D and Mu_A states are separated by an energy barrier V (and V') on the frame of configuration coordinate (Fig. 2a), then Mu can take two corresponding electronic states as initial states at low temperatures ($V, V' \gg k_B T$). The yield of each state is proportional to the relative density of states which also depends on temperature (see Appnd. C). Recently, an attempt has been made to evaluate this potential from experimentally observed yields of Mu^0 and Mu^+ in Lu_2O_3 , assuming that the relative yields of these states are determined by the potential similar to that shown in Fig. 2a, within a short time from muon stopping ($\sim 10^{-12}$ s) to the completion of the lattice relaxation ($\sim 10^{-10}$ s) [42]. When $V \leq 0$ or $V' \leq 0$, only one of these will be realized as the initial state, and its ionization is observed with increasing temperature. Since such initial states cannot be readily realized in an experiment for H under normal conditions, it is a major advantage of Mu study to allow the direct access to donor/acceptor levels ($E^{\pm/0}$).

IV. MU IN INSULATING/SEMICONDUCTING OXIDES

A. Typical electronic structure of Mu-containing defects revisited from the viewpoint of ambipolarity

In oxides with strong ionic bonding, the bottom of the conduction band consists mainly of the cation *s* band and the top of the valence band consists of the *2p* band of oxygen. Therefore, Site-D and -A in Fig. 1 can be qualitatively understood as the state of Mu governed by the interaction with the ligand oxygen (O^{2-}) and cation (K^{n+}), respectively. The schematic local structure of Mu specifically assumed here is shown in Fig. 3. The typical state at Site-D is that associated with the formation of OH bonds with oxygen by interstitial Mu (Fig. 3b–d). If we consider the molecular orbitals in Fig. 3a, the bonding orbital between O *2p* and Mu *1s* (σ_D) is filled with two covalent electrons and sinks to a deep position in the valence band, while the antibonding orbital (σ_D^*) is pushed up to the conduction band.

The state of the remaining one electron is determined by the hybridization of the σ_D^* orbital and the conduction band, and if the hybridization with *s-p*-like orbitals is strong, the electron enters the bottom of the conduction band (E_c), which contributes to conductivity regardless of temperature; $\text{O}^{2-} + \text{Mu}^0 \rightarrow \text{OMu}^- (= \text{Mu}_D^+) + e^-$ (Fig. 3b). Meanwhile, when the

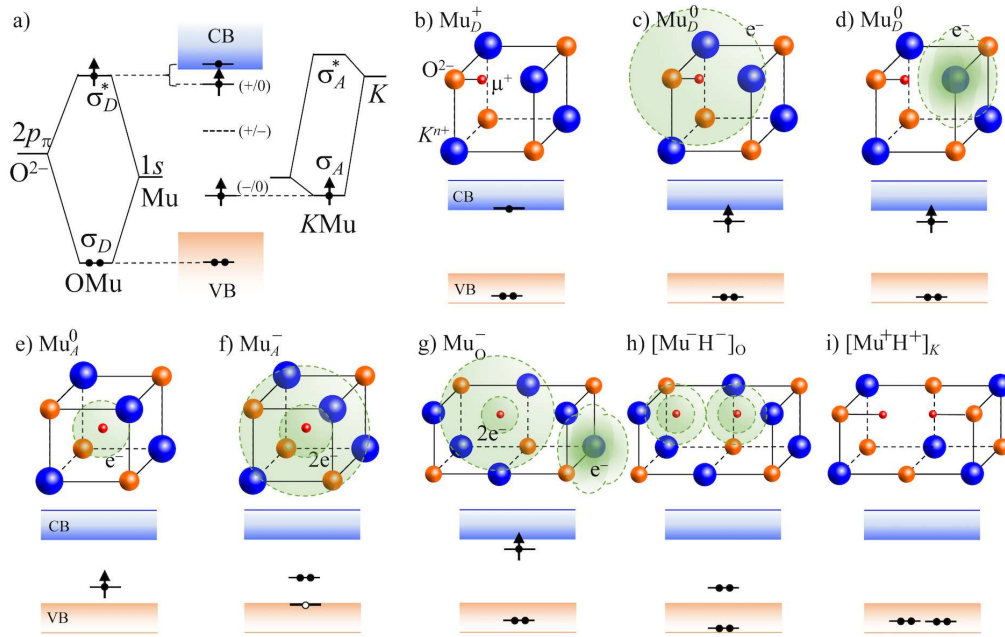


FIG. 3. a) Schematic illustration of the relationship between electronic levels and band diagrams in oxides based on molecular orbitals with Mu forming chemical bonds with oxygen (left) or cations (right). b–i) Typical defect structures involving Mu and the associated electronic states; those in b–d) indicate the states where OMu bonds are formed (Mu_D in Fig. 1b), e–f) indicate the states where Mu forms multiple bonds with cations (Mu_A in Fig. 1b), g–h) indicate complex states involving oxygen defects, and i) indicates that associated with divalent cation vacancies. d) and g) are polaron states, where electrons are localized in cationic electron orbitals (e.g., d orbitals). b–d) and g) can have n -type activity, whereas e–f) can be p -type active.

band gap ($E_g \equiv E_c - E_v$) is large and hybridization is weak, Mu strengthens the character of the isolated center and E^{+0} is formed within the gap (Fig. 3c, d). Even in this case, when E^{+0} is close to the bottom of the conduction band ($E_c - E^{+0} \lesssim k_B T$), the bound electron of Mu_D^0 is thermally excited to the conduction band at a finite temperature, and the valence state change is observed at elevated temperatures.

On the other hand, in the case of Site-A in Fig. 3a (right), Mu is surrounded by cations (see also Fig. 3e). This state is expected to be stabilized by the formation of multiple bonding with cations [11] (and/or by the antibonding character of hybridization with oxygen $2p$ band, as discussed for H_i^0 in alkali halides), accompanying the acceptor level. The electron can enter the KMu molecular bond orbitals, and serves as an acceptor; when the associated bond level (σ_A) is close to the valence band ($E^{-/0} - E_v \lesssim k_B T$), Mu is promoted to a hydride-like state by accommodating the second electron and supplying a hole to the valence band top (Fig. 3f), i.e., $\text{KMu}^0 \rightarrow \text{KMu}^- (= \text{Mu}_A^-) + h^+$. When the corresponding electron level is situated near the center of the gap, Mu is observed as an atomic Mu_A^0 . As discussed below, the Mu^0 states observed in wide-gap oxides exhibiting large hyperfine parameters are interpreted as this state, where the multipolar interaction with cations is weakest. The equilibrium charge-transition level $E^{+/-}$ is located in the middle of E^{+0} and $E^{-/0}$.

The study of Mu in oxides began on insulators with large E_g , such as SiO_2 [43, 44], Al_2O_3 [45], or MgO [44, 46], where

atomic Mu^0 states were observed with hyperfine interactions as large as that in vacuum [$|A| = A_{\text{vac}} = 4463.30$ MHz, see Eq. (20) in Appnd. B]. In subsequent studies, atomic Mu^0 has been observed almost without exception in insulators with E_g generally above 6–7 eV [47–52]. However, there are two problems in understanding these experimental results. One is that, as we have already discussed, H^+ or H^- is always more stable than H^0 irrespective of E_F due to its ambipolarity, which is inconsistent with the fact that Mu^0 is observed (given that Mu were also in thermal equilibrium). Another point is that in many of these materials, the diamagnetic Mu (Mu^+ or Mu^-) is observed to coexist with Mu^0 (e.g., in SiO_2 , the yields of Mu^0 and Mu^\pm are $\sim 65\%$ and $\sim 35\%$, respectively [44]), but the origin of these diamagnetic components remains to be identified.

These two problems can be resolved by considering that the observed electronic states of Mu correspond to the non-equilibrium states near $E^{\pm/0}$, and that Mu can simultaneously take on donor- and acceptor-like states shown in Fig. 3. In the case of SiO_2 , the position of $E^{\pm/0}$ inferred from DFT calculations for H suggests that the diamagnetic state and Mu^0 state correspond to Mu_D^+ (Figs. 3b) and Mu_A^0 (Figs. 3e), respectively (see Section IV B for more details).

In contrast to the above, the first example of Mu^0 with a “shallow donor level” ($0 < \epsilon_+ \ll E_g$) was found relatively recently in ZnO [53, 54]. This discovery was made in response to the prediction of an *ab initio* DFT calculation where both $E^{+/-}$ and $E^{\pm/0}$ lied ~ 0.4 eV below E_c [55], leading to the widespread search for shallow donor H/Mu in oxides. Ac-

According to the earlier report of the μ SR study on powder ZnO samples, a single Mu^0 state was observed with the hyperfine parameter described by $A(\theta, \phi) = A^* + D\cos^2\theta$ with $A^* = 0.50(2)$ MHz and $D = 0.26(2)$ MHz, respectively [53]. Here, θ (ϕ) is the polar (azimuthal) angle with respect to the symmetry axis of A [see Eq. (24) in Appnd. B for more details].

Apart from the fact that the values of A^* and D are comparable and thus the hyperfine interaction is clearly anisotropic, the value of A^* is orders of magnitude smaller than that of atomic Mu^0 in vacuum ($A^*/A_{\text{vac}} \simeq 10^{-4}$), leading to the consensus that the electronic state is qualitatively understood by the effective mass model with a large Bohr radius [corresponding to Fig. 3c, see Eq. (21) in Appnd. B]. Here, in order to quantitatively evaluate the origin of the hyperfine interaction, we consider the Fermi contact term A_c and the dipole field A_d from the localized moment on the symmetry axis, so that the hyperfine parameters are expressed in the following form,

$$A(\theta, \phi) = A_c + \frac{A_d}{2}(3\cos^2\theta - 1), \quad (6)$$

where the second term corresponds to the case where the principal axis of the tensor \hat{A}_d representing the dipole field from the electron is taken in the z direction [see Eq. (17) in Appnd. B]. Then, from the relations $A^* = A_c - A_d/2$ and $D = 3A_d/2$, we obtain $A_c = 0.579(9)$ MHz and $A_d = 0.177(5)$ MHz. These values suggest that the electrons associated with Mu^0 are rather close to the intermediate situation between Figs. 3c and d. Here, the electron responsible for A_d is assumed to be in the $4s$ orbital of Zn with considerable degree of delocalization. The fact that A_d takes a value comparable to A_c suggests the formation of an off-center polaron state in which the centers of positive and negative charges do not match.

Subsequent measurements on single crystals revealed that there were two different Mu^0 states, where the angular dependence of the hyperfine interaction was isotropic with respect to the rotation of the crystal (wurtzite type) around the $\langle 0001 \rangle$ axis. This suggests that the local structure of these two Mu^0 states respectively correspond to the bond-center and antibonding positions along the Zn-O bond that is parallel with the $\langle 0001 \rangle$ axis [54] in line with theoretical predictions [55]. Looking back from the viewpoint of ambipolarity, the two observed states may correspond to donor/acceptor-like states, where the bond-center Mu^0 is tentatively assigned to Mu_D^0 , and another situated at the antibonding position surrounded by Zn to Mu_A^0 . This also rises an additional issue on the origin of the diamagnetic state coexisting with these two Mu^0 states at low temperatures, which is discussed later (see Sect. IV C).

The Mu^0 state accompanying a shallow donor-like state observed in TiO_2 (rutile) is a typical example corresponding to the limit of the off-center polaron state ($A_d \gg A_c$, Fig. 3d). This is a complex state involving Mu, O, and Ti in which the accompanying electron is loosely localized in the $3d$ -orbitals of neighboring Ti atom(s) [56, 57]. An earlier ENDOR study reported the H-related paramagnetic center with a similar electronic structure in a reduced sample [58]. In

such an electronic state, the hyperfine interaction is dominated by the magnetic dipole interaction [the second term of Eq. (6)], so that the hyperfine parameters may satisfy the relation $\text{Tr}\hat{A}_d = 0$. In fact, this relationship is nearly satisfied for TiO_2 , although there are slight differences among the literature [56–58]. Notably, the size of the localized moment estimated from A_d is only about $\sim 0.05\mu_B$, and it is highly likely that the state is more extended (larger polaron-like, or of greater distance between Mu^+ and e^-). Moreover, the emergence of the second Mu^0 states with a greater A_d below ~ 5 K coexisting with the diamagnetic state [57] recalls the situation in ZnO. Recent studies on Mu in SrTiO_3 have also reported electronic states similar to TiO_2 [59], where the localized moment at the Ti site is as large as $\sim 0.33\mu_B$, suggesting a more strongly localized state (small polaron-like) than that in TiO_2 .

Interestingly, all of the charge transition levels ($E^{+/-}$, $E^{-/0}$, and $E^{+/0}$) for H in ZnO, TiO_2 , and SrTiO_3 inferred from previous first-principles DFT calculations lie within the conduction band [11, 55, 60]. The naive application of our model to those oxides would predict only Mu^+ , which is in contrast to the experimental observations. These disparities have previously been considered as individual anomalies in view of the relative accuracy of the DFT calculations, but we will show in Sect. IV C that considering the polaronic state leads to an alternative model for the origin of these shallow levels.

For the sake of completeness, let us now consider the complex state with atomic vacancies. The requirement for stabilizing hydride states is expected to be readily satisfied in oxygen vacancies (V_O^{2-}). When their concentration is sufficiently high, Mu may also have a chance to be trapped there to form various local electronic states. For H, it is theoretically predicted that one or two H^- ions are accommodated in a single oxygen vacancy. While the hydride state for the interstitial Mu/H is attained by capturing an electron to the acceptor levels, the single Mu^-/H^- atom trapped in V_O^{2-} can be donor-like due to the occurrence of the excess electron, e.g., $\text{Mu}^0 + \text{V}_O^{2-} \rightarrow [\text{Mu}^-]_O + e^-$, where $[]_O$ denotes the oxygen substitutional site (see Fig. 3g). The donor-like behavior of $[\text{H}^-]_O$ is known to be crucial for the realization of high electron doping by O substitution with H, e.g., in iron-based superconductors [61].

On the other hand, when two H^- ions are included, as in Fig. 3h, passivation by charge compensation occurs. This may be equivalent to the formation of metal hydrides. As already mentioned in Sect. II, the probability of two Mu atoms coming into close proximity under practical experimental conditions is negligibly small. But in situations where there are many oxygen vacancies containing a single H^- , Mu is expected to have a good chance of finding such a site. This allows Mu to form a Mu-H complex defect to passivate the electrical activity ($\text{Mu}^0 + [\text{H}^-]_O + e^- \rightarrow [\text{Mu}^-\text{H}^-]_O$). In fact, recent muon experiments performed on amorphous $\text{InGaZnO}_{4-\delta}$ doped with large amounts of H (a-IGZO:H) have found evidence for the formation of such a state [62]. The μ SR spectra observed in IGZO without H-doping, regardless of whether it is crystalline or amorphous, show depolarization described by a Gaussian Kubo-Toyabe function of the diamagnetic Mu [Eq. (15) in

Appnd. A], implying that Mu feels a Gaussian random local fields induced by a number of In/Ga nuclear magnetic moments at nearly equal distances. In contrast, those in a-IGZO:H exhibit a Lorentzian lineshape with an enhancement in the depolarization rate, strongly suggesting the presence of H in addition to In/Ga nuclei at the nearest neighbor of Mu. The latter is in line with the formation of $[\text{Mu}^-\text{H}^-]_{\text{O}}$ complex state in a-IGZO:H, where the associated electronic levels are predicted to lie just above the valence band top to accommodate two electrons (see Fig. 3h) [62, 63]. These levels are the prime suspect of the negative bias illumination stress (NBIS) instability for a-IGZO [64–66], where the instability is essentially a persistent photoconductivity caused by the photo-excitation of these electrons into the conduction band. A similar $[\text{Mu}^-\text{H}^-]_{\text{O}}$ complex state has been reported in partially hydrated $\text{BaTiO}_{3-x}\text{H}_x$ [67, 68].

More interesting point in IGZO from the viewpoint of ambipolarity is that the role of H varies qualitatively with its concentration. As mentioned above, Mu in crystalline and as-deposited amorphous thin films does not form a Mu^0 state regardless of temperature. Based on a comparison of the observed magnitude of the μSR linewidth Δ [proportional to the mean square of the random field from the nuclear magnetic moments $\langle |\mathbf{H}_d|^2 \rangle$, see Eq. (13) in Appnd. A] and the Δ predicted for the stable site by DFT calculations, the Mu site was narrowed down to be located in the bond center of ZnO, taking the Mu^+ state [62]. This means that the local electronic structure of isolated Mu/H in IGZO is represented by that shown in Fig. 3b, which is evidence that H behaves as an n -type impurity regardless of temperature in the limit of dilute concentration. Thus, the ambipolar property of H allows itself to play the roles of donor- and acceptor-like defects, determined by the local atomic structures that depend on the H concentration.

Finally, regarding the relationship with the cation vacancy, H/Mu serves to compensate the oxygen dangling bonds. Mu may be found together with other protons in multivalent cation vacancies; e.g., $[\text{Mu}^+\text{H}^+]_{\text{K}}$ (see Fig. 3i). This, for example, corresponds to the state known as the Ruetschi proton in manganese oxides [69, 70]. A recent muon study on rutile-type MnO_2 ($\beta\text{-MnO}_2$) suggests that about 15% of the implanted Mu are involved in (or located near) the $[4\text{H}^+]_{\text{Mn}}$ complexes, while the remaining 85% are in the diamagnetic state (OMu^-) at the oxygen channels [71]. In this study, hydrogen-sensitive temperature-desorption measurements revealed that as-prepared MnO_2 sample contains a considerable amount of H ($\simeq 3 \times 10^{19} \text{ cm}^{-3}$), indicating that hydrogen impurity can be the origin of the conductivity of $\beta\text{-MnO}_2$ which is presumed as an insulator ($E_g \simeq 0.04\text{--}0.17 \text{ eV}$)

B. Electronic state of implanted Mu determined by $E^{+/0}$ and $E^{-/0}$

The results of DFT calculations performed to date on the interstitial H in various oxides can be qualitatively classified into four patterns in terms of the E_F dependence of $E^q(E_F)$, and the relationship between $E^{+/-}$, $E^{\pm/0}$ and the band structure,

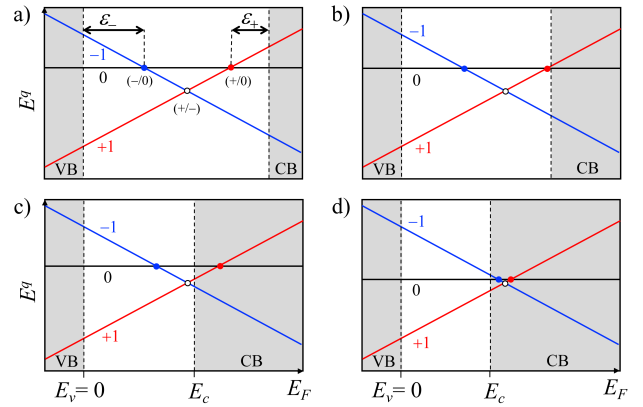


FIG. 4. Fermi level dependence of the formation energy E^q of the charged state $q (= 0, \pm 1)$ obtained by DFT calculations for interstitial H in oxides. The symbols $(+/-)$ and $(\pm/0)$ correspond to the mutual intersection points of E^q ($E^{+/-}$ and $E^{\pm/0}$). The electrical activity of H is determined by the relationship between $E^{+/-}$ and E_c and E_v , whereas that of Mu is governed by $E^{\pm/0}$ and is predicted by the sign and value of ϵ_{\pm} (see text).

as indicated in Fig. 4. Provided that $E^{+/-}$ serves as the pinning level for E_F (i.e., a considerable amount of H is present), the electric activity of H is determined by the relationship between $E^{+/-}$ and E_c (measured from $E_v = 0$). Fig. 4a-b shows the deep $E^{+/-}$ level, Fig. 4c shows the shallow $E^{+/-}$ level, and Fig. 4d shows that there is no level in the gap and only H^+ is stable. Interestingly, early DFT calculations proposed a model in which $E^{+/-}$ is aligned at a certain energy measured from the vacuum level ($E^{+/-} - E_{\text{vac}} \sim -3 \text{ eV}$) regardless of oxides [72]. This model has been also applied to the cases of Mu in the literature [47, 73], and the existence of shallow donor levels have been predicted in Bi_2O_3 , HgO , Sb_2O_3 , and so on, in which no such state has been actually observed. However, as already mentioned, a coherent interpretation becomes possible for Mu by considering E_F vs $E^{\pm/0}$ instead of $E^{+/-}$ and that Mu is in the relaxed-excited states related with $E^{\pm/0}$.

A seminal example for the importance of considering $E^{\pm/0}$ is the early studies of Mu in strongly covalent semiconductors, where both donor- and acceptor-like Mu^0 states (respectively corresponding to Mu_D^0 and Mu_A^0 in Fig. 1b) have been observed to coexist [1, 38]. Interpreting the charge changes of Mu_D^0 and Mu_A^0 as respectively associated with $E^{+/-0}$ and $E^{-/0}$, and estimating $E^{+/-0}$ by their interpolation using Eq. (2), it was found that $E^{+/-}$ was situated near the charge neutral level (E_{CNL}) common to materials in question [74]. In this study, the authors focused on whether the position of $E^{+/-}$ is independent of the material (see Sect. IV E for details), but the results support that the change transition (ionization) of Mu^0 depends on the $E^{\pm/0}$ level rather than $E^{+/-}$; note that $E^{\pm/0}$ were also in semi-quantitative agreement with the predictions of DFT calculations [75]. Let us now investigate whether a coherent understanding of the Mu valence state in oxides is attained by this presumption.

In the left column of Table I, the experimental results of

Mater.	Exp. [E_g (eV)]			DFT Calc. [$E_g, E^{+/-}, E^{\pm/0}, \varepsilon_{\pm}$ (eV)]						
	E_g	Mu	Refs.	E_g	$E^{-/0}$	$E^{+/-}$	$E^{+/0}$	ε_{\pm}	Mu	Refs.
BeO	10.6	Mu_X^0	[47, 48]	10.6	5.5	6.09	6.7	3.9	$\text{Mu}_{A/D}^0$	[48]
SiO ₂	9.0	$\text{Mu}_X^0, \text{Mu}^+$	[43, 44]	8.7	2.9	5.4	7.9	0.8	$\text{Mu}_A^0, \text{Mu}_D^0$ ★	[11]
α -Al ₂ O ₃	8.8	$\text{Mu}_X^0, \text{Mu}^+$	[45, 76]	8.5	3.0	5.4	7.7	0.8	$\text{Mu}_A^0, \text{Mu}_D^0$ ◆	[11]
MgO	7.8	$\text{Mu}_X^0, \text{Mu}^+$	[44, 46]	7.5	2.8	5.4	7.9	-0.4	$\text{Mu}_A^0, \text{Mu}_D^+$	[11]
m-HfO ₂	6.0	$\text{Mu}_X^0, \text{Mu}^+$	[49]	5.8	1.6	4.0	6.3	-0.5	$\text{Mu}_A^0, \text{Mu}_D^+$	[11]
q-GeO ₂	6.0	$\text{Mu}_X^0, \text{Mu}^+$	[44, 47]	5.6	2.0	4.8	7.2	-1.6	$\text{Mu}_A^0, \text{Mu}_D^+$	[11]
Lu ₂ O ₃	5.6(1)	$\text{Mu}_X^0, \text{Mu}^+$	[52]	4.0	1.1	2.46	4.2	-0.2	$\text{Mu}_A^0, \text{Mu}_D^+$	[52]
ZrO ₂	5.5(3)	$\text{Mu}_X^0, \text{Mu}^+$	[50]	5.4	2.1	3.5	4.8	0.6	$\text{Mu}_A^0, \text{Mu}_D^+$ ★	[77]
Y ₂ O ₃	5.5	$\text{Mu}_A^0, \text{Mu}^+$	[51]	5.9	2.15	3.8	5.5	0.4	$\text{Mu}_A^0, \text{Mu}_D^+$ ★	[51]
La ₂ O ₃	5.4(1)	$\text{Mu}_X^0, \text{Mu}_S^0$	[47]	5.2	0.3	3.0	6.2	-1	$\text{Mu}_A^0, \text{Mu}_D^{\parallel}$	[11]
β -Ga ₂ O ₃	5.0	Mu^+	[78]	4.8	3.2	4.9	6.4	-1.6	Mu_D^+	[11]
c-IGZO	3.68	Mu^+	[62]	3.1	>3.1	>3.1	4.8	-1.7	Mu_D^+	[63]
SnO ₂	3.6	Mu^+	[47, 79]	3.6	4.1	4.3	4.6	-1	Mu_D^+	[11]
ZnO	3.4	$\text{Mu}_S^0, \text{Mu}^+$	[53, 54]	3.4	≥ 3.4	≥ 3.4	3.4	0	Mu_D^{\parallel}	[80]
α -TeO ₂	3.4	$\text{Mu}_A^0, \text{Mu}^+$	[81]	2.82	0.8	2.2	2.82	0	$\text{Mu}_A^0, \text{Mu}_D^+$	[81]
SrTiO ₃	3.2	$\text{Mu}_S^0, \text{Mu}^+$	[59, 82]	3.1	>4	3.8	3.5	-0.4	Mu_D^{\parallel}	[60, 83]
r-TiO ₂	3.2	$\text{Mu}_S^0, \text{Mu}^+$	[56, 57]	3.0	2.6	3.1	3.5	-0.5	Mu_D^{\parallel}	[11]
In ₂ O ₃	2.7(1)	Mu^+	[79]	2.67	1.8	3.2	3.67	-1	Mu_D^+	[84]
w-GaN	3.48	$\text{Mu}_S^0, \text{Mu}^+$	[85]	3.4	1.2	2.4	3.5	-0.1	Mu_D^{\parallel}	[86]

TABLE I. Comparison between the valence state of Mu in various oxides and DFT calculations for the interstitial H. $E^{\pm/0}$, $E^{+/-}$ are the energy with E_V as the origin ($E^{-/0} = \varepsilon_-$). Mu_X^0 refers to the deep level Mu^0 [corresponding to either donor ($X = D$) or acceptor ($X = A$) in DFT calculations], and Mu_S^0 to the shallow donor level Mu^0 . For these marked by ★, the discrepancy can be attributed to $E^{+/-}$ over indirect gaps around the Γ point (see text and Fig. 5) or to the ambiguity in the experimental background mimicking Mu^+ signal, while those marked by \parallel exhibits a correlation with the polaronic (off-center) Mu_S^0 . For the case of α -Al₂O₃ (marked by ◆), see text.

Mu in several oxides for which DFT calculations have been performed are listed in descending order of the magnitude of E_g , and the observed electronic states of Mu are shown. The corresponding energies E_g , $E^{\pm/0}$, and ε_{\pm} (see Fig. 4a for the definition) obtained by DFT calculations are shown in the right column. These compounds comprise a subset of oxides in which the conduction and valence bands consist of empty cation ns^0 and O $2p$ orbitals (represented by Fig. 3a). Fig. 5 shows $E^{\pm/0}$ vs band structure, where all the energy levels are aligned to the vacuum level by considering the electron affinity [11]. Although it is not explicitly shown in Fig. 4, the local structures of Mu corresponding to $E^q(E_F)$ can be different between $q = +1$ and -1 (e.g., Y₂O₃ [51]). Therefore we refer to Mu_D^+ and Mu_A^- according to Figs. 3b–f, respectively. The electronic state of Mu observed in the vicinity of $E^{+/0}$ is then assigned to $\text{Mu}_D^0/\text{Mu}_D^+$, and that in the vicinity of $E^{-/0}$ is to $\text{Mu}_A^0/\text{Mu}_A^-$. Based on the comparison between the $E^{\pm/0}$ levels and band structures (which are visualized in Fig. 5), the second column from the right predicts the state of Mu observed as the initial state at low temperatures. Provided that the transition barrier between Mu_D and Mu_A (V, V' in Fig. 2) is sufficiently large, both Mu_D^0 and Mu_A^0 may be observed for the case of $\varepsilon_+ > 0$ and $\varepsilon_- > 0$ (Fig. 4a–b), Mu_A^0 and Mu_D^+ for $\varepsilon_+ < 0$ and $\varepsilon_- > 0$ (Fig. 4c), and only Mu_D^+ for the case of Fig. 4d. (When V or $V' \leq 0$, only Mu_D or Mu_A are observed.)

It is clear from the left columns in Table I that Mu^0 with large hyperfine parameters are observed simultaneously with diamagnetic states in oxides with E_g greater than ~ 5 eV (ex-

cept for BeO), which can be attributed to the Mu_A^0 and Mu_D^+ states that accompany $E^{-/0}$ and $E^{+/0}$, respectively (corresponding to Fig. 4b or 4c). Among those in which the calculated $E^{+/0}$ is in the band gap to predict Mu_D^0 states (★ in the Table I), SiO₂, ZrO₂, and Y₂O₃ have indirect gaps smaller than E_g around the Γ point in the energy band structure, where the bottoms of the dispersive bands extend below (or near) $E^{+/0}$ [51, 87, 88]. The dashed parabolic curves found in Fig. 5 symbolically represent the energetic extent of the band dispersion around the Γ point. Thus, the diamagnetic states in these oxides are also interpreted as Mu_D^+ . (In the actual experiment, there remains a possibility that the diamagnetic signal involves contributions from background and/or a fraction of muons that missed the electrons in the initial stage, although the Mu^0 can be attributed to one of two states attained in the case of V or $V' \leq 0$.) Yet another exceptional case is α -Al₂O₃ (◆ in the Table I), for which the recent study suggests the occurrence of complex interactions between Mu, phonons, and excitons [89].

The fact that Mu^0 is also observed at ambient temperatures in these materials is consistent with DFT calculations, because they predict that $E^{-/0}$ is situated far from the valence band ($\varepsilon_- \gtrsim 1$ eV); the possibility for Mu_A^0 to change its valence state by capturing holes would be small even at ambient temperature. Note that according to the DFT calculation, BeO corresponds to Fig. 4a, and the fact that only a single Mu^0 is experimentally observed suggests the situation that V or V' is negative.

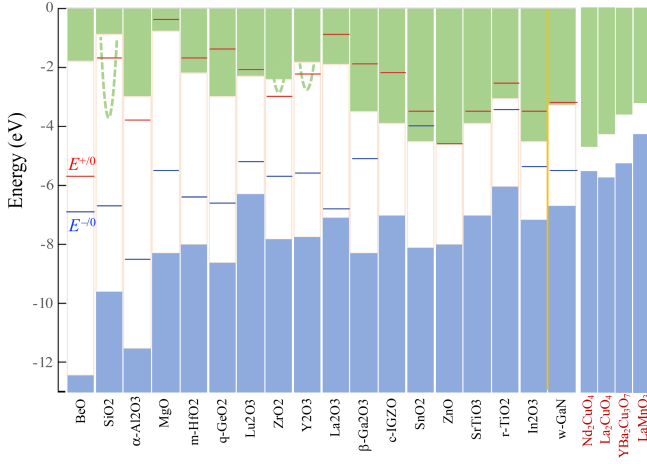


FIG. 5. The donor/acceptor levels (E^{+0}/E^{-0}) in Table I plotted on the band structure aligned to the vacuum level. The parabolic curves just beneath the conduction band minimum in SiO_2 , ZrO_2 , and Y_2O_3 indicate the presence of dispersive bands with narrower gaps around the Γ point. $E^{-/0}$ is unknown for c-IGZO, ZnO, and SrTiO_3 . (α - TeO_2 is not included because the electron affinity is unknown.) The band structure for the typical cuprates/manganites are also shown for comparison (see Sect. IV F).

Regarding the situation shown in Fig. 4c where $E^{-/0}$ is predicted to lie above the mid-gap, it is necessary to know the position of E_{CNL} for discussing whether $E^{-/0}$ can exist as an acceptor level within the band gap. However, it has been argued that E_{CNL} is almost identical with $E^{+/-}$ for H in binary compounds [75] and in oxides [11, 90], which has been in line with experimental implication for Mu in semiconductors with a relatively narrow band gap [79]. Thus, it is reasonable to assume at this stage that the condition of $E_{\text{CNL}} \simeq E^{+/-} \geq E^{-/0}$ holds for H/Mu in general. This can also be rephrased that hydrogen, with its ambipolarity, is a probe of the charge neutral level through its own charge state.

In contrast to the case of wide-gap oxides, the predicted E^{+0} levels in those with a band gap of less than ~ 5 eV fall in the conduction band ($\epsilon_+ \leq 0$) without exception. Moreover, the $E^{-/0}$ level is deep in the gap (large value of ϵ_-), merging to E^{+0} with decreasing E_g (except for β - Ga_2O_3 and In_2O_3). Therefore, only the Mu^+ state is considered to be stable in these materials. However, there are a number of cases where the Mu^0 state, which is regarded as a shallow donor, is observed experimentally. We will argue in the next section that these can be understood consistently by considering a common feature that the Mu^0 state exhibits polaron-like features, and by taking into account the strong electron-phonon coupling exhibited by the host.

C. Polaron states mimicking donor-like Mu

The electronic state of Mu^0 that behaves like a shallow donor (abbreviated as Mu_S^0 , which is observed in oxides with $E_g \lesssim 5$ eV) is spatially extended, and its electronic structure can be discussed from the anisotropy of hyperfine interac-

tions. As already mentioned in Section IV A, those in ZnO, TiO_2 , and SrTiO_3 studied so far all exhibit an off-center polaronic character. The values of the hyperfine parameters in these materials are summarized in Table II, where they are expressed by applying Eq. (6). In each case, A_d is comparable to or greater than A_c , suggesting that the simple effective mass model of atomic H with a large Bohr radius is not suitable for understanding such electronic structures.

Interestingly, these electronic states show distinct similarities to the off-centered STE in alkali halides consisting of the hole localized on a halogen dimer (X_2^- , known as V_k centers) and the electron at the halogen vacancy (corresponding to the F center) situated next to the X_2^- dimer [18, 19, 91, 92]. If we consider OMu^- as an analogue of the hole-localized halogen dimer, then the electron attracted to it is presumed to avoid the Coulomb repulsion from the nearby anions, being localized at the cation. Thus, the electronic structure of Mu_S^0 can be interpreted as a result of compromise among the strong electron-phonon coupling that promotes the localization of electrons, the Coulomb attraction from Mu^+ , and the Coulomb repulsion from the neighboring O^{2-} . In other words, Mu_S^0 is an STE-like state involving Mu, mimicking the shallow donor Mu_D^0 state.

This similarity suggests that the Mu-exciton interaction discussed at the beginning also contribute to the formation of Mu_S^0 , while the local charge polarity of $\text{OMu}^- (= \text{Mu}_D^+)$ is opposite to the interstitial Mu_A^+ . In fact, excitons bound to various donor/acceptor impurities are known to exist in ZnO and TiO_2 , and their local electronic structure has been investigated by photoluminescence spectroscopy [93–95]. A very recent report provides a variety of H-related bound excitons in ZnO [96], although that corresponding to the bond-center H^0 seems missing (probably due to the small yield). Therefore, the polaron-like bound states observed in these materials can be qualitatively understood, including the reason for the off-centered electronic structure, by adopting a reversed viewpoint that OMu^-/OH^- serves as an electron trap to form a complex state analogous to the donor-bound exciton [30].

We have long been plagued by the problem that the $E^{+/-}$ levels obtained by DFT calculations for these oxides not only contradict the observation of neutral Mu^0 states, but also do not correspond to “shallow” donor levels. Our new model provides a fundamental shift from such a naive interpretation in that the shallow donor-like Mu^0 corresponds to a relaxed-

	A_c (MHz)	A_d (MHz)	Refs.
ZnO	0.579(9)	0.177(5)	[54]
	0.436(12)	0.286(7)	
TiO_2	-0.06(5)	0.86(6)*	[56]
SrTiO_3	1.4(3)	15.5(2)	[59]
GaN	0.079(22)	0.258(22)	[85]

(* $0.05\mu_B$ on the nearest neighbor Ti)

TABLE II. Fermi contact term (A_c) and magnetic dipole interaction (A_d) in Mu^0 [see equation (6)]. For ZnO, two states ($\text{Mu}_{1,2}$) have been observed from μSR experiments on single crystals, and the values for each are given.

excited state, where the bound state is formed by the capture of the exciton electron to the E^{+0} level with the help of strong electron-phonon interactions.

The localization of electrons is promoted by the electron-phonon coupling, which has been inferred to be strong in ZnO [97], TiO₂ [98], and SrTiO₃ [99] from the suppression of electron mobility at higher temperatures. In contrast to these cases (including ZnO), a monotonous enhancement of carrier mobility is observed with increasing temperature in the pristine a-IGZO [100], in which no shallow state is observed for Mu localized near the Zn-O bond center [62]. Thus, considering that the local atomic configuration of Mu/H is almost identical between ZnO and IGZO [62], the strong electron-phonon coupling is another important factor to enhance the localization of electrons around the OMu⁻ complex. This invokes the precaution that the activation energy for the promotion from Mu_D⁰ to Mu_D⁺ cannot be simply attributed to ε_+ ; it includes the contribution of the adiabatic potential barrier for the electron between the localized state and the continuous state [59]. (A similar argument would be the case for α -Al₂O₃ in the previous section.) The effect of the electron-phonon coupling has also been theoretically investigated in terms of the duality of the conduction band carriers in TiO₂ and SrTiO₃, which can be in both the continuous state and the deep level (self-trapped) state in the gap [101].

In any case, when the donor-like Mu⁰ (Mu_D⁰) is observed experimentally despite that the DFT calculation predicts E^{+0} is in the conduction band ($\varepsilon_+ \lesssim 0$), the possibility of electron localization at Mu_D⁺ enhanced by the electron-phonon coupling is plausible as the primary cause. It should be pointed out that this is also likely for the “shallow donor Mu⁰” observed in GaN [85], for example (bottom row of Table I). Previous theoretical calculations have predicted that $\varepsilon_+ \sim 0$, and that interstitial H in GaN does not form shallow donor levels as described by the effective mass model [8]. (That the electronic state of Mu was discussed in relation to $E^{+/-}$ which was located deep in the band gap was also the problem.) In contrast, the reported hyperfine interaction has c -axis symmetry with $A_{\parallel} = 0.337(10)$ MHz and $A_{\perp} = -0.243(30)$ MHz. Deriving the parameters of Eq. (6) from these values gives the values shown in Table II, indicating that the magnetic dipole interaction is dominant, as in the case of TiO₂. The presence of strong electron-phonon coupling has been inferred from the suppression of the hole mobility in GaN at high temperatures [102]. Furthermore, the occurrence of H-exciton interaction has been also demonstrated by photoluminescence spectroscopy [103]. These situations suggest that Mu⁰ in GaN can be also understood as analogous to a donor-bound exciton in which an electron is localized near Mu_D⁺ by electron-phonon coupling to mimic the shallow donor state.

Now, provided that the bound-exciton model properly explains the Mu_S⁰ state, it is expected that the localization of electrons in the vicinity of Mu will be determined by stochastic processes which may be also influenced by the presence of other impurities and defects nearby. Therefore, the diamagnetic states in these oxides can be attributed to the Mu_D⁺ state predicted by the DFT calculation, where the relative yield between Mu_S⁰ and Mu_D⁺ is presumably determined by the local

carrier (exciton) density.

At this stage, it may be worth a comment on the claim for the existence of Mu⁰ with shallow levels in SnO₂ [47, 79]. The reported hyperfine parameter is as small as $A/2 = 0.045(1)$ MHz with small relative yield ($\sim 3.6\%$) [79], and it is not clear how it was distinguished from slow depolarization due to nuclear magnetic moments ($\Delta \simeq 0.03$ MHz [47]) and its apparent reduction due to muon diffusion (that mimics the promotion of Mu⁰ to Mu⁺). In any case, the important point is that the majority of implanted Mu is in a diamagnetic state, which can be attributed the donor-like Mu⁺ state.

Recently, a detailed comparison between the magnitude of the internal magnetic field at the Mu position observed in the magnetically ordered phase of Cr₂O₃ and Fe₂O₃ (which contain magnetic ions) and the local electronic state predicted by DFT calculations shows that the electrons associated with Mu are localized in the $3d$ -orbitals of the Cr/Fe ions [104, 105]. Since the electron-phonon coupling is known to be strong in these materials, these off-centered electronic states indicate that a similar mechanism is at work in the formation of polarons.

D. Fast diffusion of acceptor-like Mu

It is expected that the donor-like Mu in non-metallic compounds (Mu_D) forms a covalent bond (σ bond) with anions and requires relatively large activation energy to migrate between the equivalent sites, whereas many examples of fast diffusive motion of Mu⁰ have been reported. In elemental semiconductors (Si, Ge), macroscopic diffusion coefficients have been inferred for Mu_A⁰ (the “normal muonium”) occupying the center of the tetrahedral interstitial position (the T_d site) [74] through the diffusion-limited trapping of Mu⁰ to extrinsic impurities [38]. The detailed temperature dependence of the hopping frequency of Mu⁰ has been revealed via the dynamical fluctuations of the nuclear hyperfine interaction (i.e., that between nuclear spins and an orbital electron of Mu⁰ [38]). Figure 6 shows an example in GaAs [31, 106], where the relevant Mu⁰ state was later inferred to be located at the center of the cationic Ga tetrahedral cage (i.e., Mu_A⁰) [107]. Fast hopping motion of Mu⁰ at the T_d site was also reported in diamond (C), where a qualitatively similar temperature dependence was observed [108]. Moreover, such a behavior is also suggested for the Mu_A⁰-like states in various compounds other than oxides (including iron pyrite, see the next section). These observations suggest that the acceptor-like Mu⁰ have an intrinsic property of fast diffusion in common. Here, it must be emphasized that Mu⁰ in the presence of high density carriers behave as if it is in the diamagnetic state due to the motional narrowing of the hyperfine interaction caused by the fast spin/charge exchange [109]. In such a situation, Mu diffusion can be monitored via the fluctuation of local magnetic fields exerted from nuclear magnetic moments, where the muon depolarization is described by the dynamical Gaussian Kubo-Toyabe function [110].

In general, Mu/H in solid crystals is presumed to form a polaronic state in itself due to the interaction with the lattice

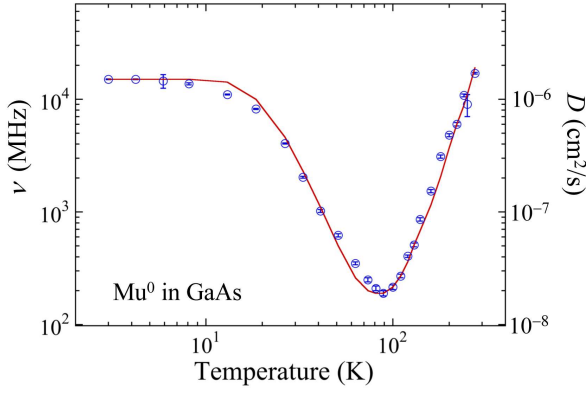


FIG. 6. Temperature dependence of Mu_A^0 hopping frequency (ν) observed in GaAs, where the solid curve represents theoretical prediction by the quantum diffusion model (after Ref.[31]). The corresponding diffusion constant (D) is derived from the relationship $D = a^2 \nu / 32$ (with $a = 0.56535$ nm being the lattice constant).

(phonons), and the self-diffusion is well understood by the hopping motion of small polarons [111]. From the previous discussion on the electronic state of H_i^0 in alkali halides, the antibonding character of acceptor-like Mu/H with surrounding anions emerges as an additional factor to enhance the isolation of Mu_A^0 . Because of the light mass, the tunneling effect is known to dominate the hopping frequency of Mu/H even at ambient temperatures. The high symmetry of the local structure around Mu_A^0 stemming from the antibonding character seems to be advantageous for having a relatively large tunneling matrix.

More specifically, there are two modes of tunneling motion: one is the thermally activated tunneling, in which thermal excitations (phonons) enhances tunneling by compensating the self-trapping energy (phonon-assisted tunneling), and another in which phonons inhibit the intrinsic (coherent) tunneling by blurring the final state [112]. As shown in Fig. 6, hopping frequency increases with increasing temperature on the high temperature side ($T \gtrsim \Theta_D/3$, with $\Theta_D \simeq 347$ K being the Debye temperature of GaAs) as the phonon-assisted tunneling becomes dominant. Meanwhile, the hopping frequency increases again at low temperatures as the phonon scattering decreases with decreasing temperature, and converges to a frequency determined by the magnitude of the tunneling matrix. This behavior was first observed clearly for Mu^0 in alkali halides [113, 114], and is expected to be true for oxides as well, since similar situations are suggested for elemental semiconductors and group 13-15 compounds.

In fact, it is known that the atomic Mu^0 is emitted into the vacuum when a silica powder sample (SiO_2) placed in a vacuum is irradiated with muons [115, 116], indicating that the Mu^0 produced within SiO_2 particles (sub-micrometers in diameter) diffuses rapidly to reach the crystalline surface. In addition, motional narrowing due to fast diffusion of Mu^0 in SiO_2 above 180 K has been pointed out as the reason for the disappearance of the anisotropy in the hyperfine parameters associated with the electric quadrupole interaction of Mu^0 . Conversely, this is consistent with the interpretation of Mu^0 in

SiO_2 as an acceptor-like state (not bound to O) in the previous section. Such fast diffusion of acceptor-like Mu/H may have some implications for recent studies of hydride conduction in metal oxyhydrides [117, 118].

E. Comparison with hydrogen in thermal equilibrium

In contrast to the case of Mu, the electrical activity of H in a material of equilibrium state is considered to be determined by the position of the $E^{+/-}$ level in the energy band structure. When $E^{+/-} > E_c$, the electronic level strongly hybridizes with the conduction band and falls to the bottom of the band, and H becomes an electron donor regardless of temperature. The same is true for the electric activity as acceptors, which is determined by the relationship between $E^{+/-}$ and E_v . In addition, when $E^{+/-}$ is in the midgap ($E_v < E^{+/-} < E_c$), the hybridization is weak and the isolated H is electrically inactive. Therefore, the behavior of $E^{+/-}$, including whether or not it shows any regularity, is very important in predicting the electrical activity of H. In fact, $E^{+/-}$ in group 13-15 compound semiconductors and oxides has been vigorously evaluated by first-principles calculations in the past decades.

As mentioned earlier, it was suggested from the earlier DFT calculations that $E^{+/-} - E_{\text{vac}}$ takes a universal value common to oxides [72]. This is in stark contrast to the cases of E_c and E_v vs E_{vac} that vary among oxides without systematics. Such an alignment of $E^{+/-}$ was originally proposed for deep impurity levels in binary compound semiconductors, and it has been suggested that the local impurity-host interaction (e.g., strength of covalency) determines the depth for each class of compounds [119]. This alignment hypothesis has been applied to a series of oxides [120], from which the candidates with shallow donor levels were proposed [72].

A model was also proposed in which the alignment of $E^{+/-}$ occurs midway between the σ_D^* and σ_A bonding lev-

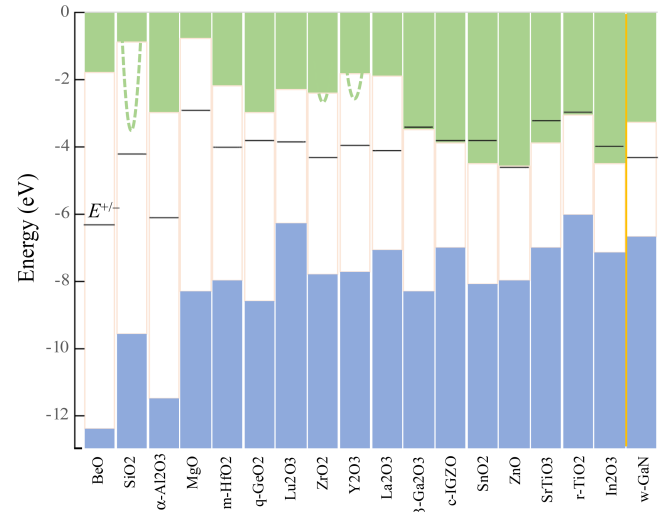


FIG. 7. The equilibrium charge-transition levels ($E^{+/-}$) in Table I plotted on the band structure aligned to the vacuum level.

els in Fig. 1a (the antibonding level raised above the conduction band by the OH bond and the O $2p$ level generated by the metal-hydrogen bond, respectively) [121, 122]. Thus $E^{+/-}$ is expected to be located near the charge neutral level ($E_{\text{CNL}} - E_{\text{vac}} \simeq -5$ eV). Assuming that E_{CNL} is at a constant offset to the top of the valence band (which mainly consists of O $2p$ orbitals), the H levels are expected to exhibit the tendency of alignment around E_{CNL} . This model also appears to account for deeper levels such as those in SiO_2 , Al_2O_3 , and MgO , which were not well explained by the previous model of offset alignment from E_{vac} . The $E^{+/-}$ levels relative to E_{vac} estimated by DFT calculations quoted in Table I are shown in Fig. 7, which are qualitatively in line with these scenarios.

These predictions about $E^{+/-}$ have aroused a great deal of interest, and the results of experimental verification studies conducted up to 2005 with special focus on shallow donor Mu levels in oxides have been reported in two review papers [47, 73]. According to them, SnO_2 , La_2O_3 , TiO_2 (rutile) exhibited shallow donor levels, and Al_2O_3 , MgO , and SiO_2 seemed to have deep in-gap levels, which were both in line with the predictions. Meanwhile, Bi_2O_3 , HgO , and Sb_2O_3 turned out to be characterized by large hyperfine parameters suggesting deep levels in contradiction to the predicted shallow donor state.

As has been already discussed in Sect. IV B, such discrepancies can be resolved by departing from the implicit assumption that the electrical activity of Mu is dominated by $E^{+/-}$ in analogy with H. (The partial success in the previous attempts can be attributed to the fact that the difference between $E^{+/-}$ and $E^{+/0}$ was relatively small in some oxides.) The electronic states of Mu in elemental (group 14) and 13-15 compound semiconductors have come to a coherent understanding by assuming that it varies with the occupancy of the $E^{\pm/0}$ levels. This also allowed to estimate $E^{+/-}$ by interpolation from $E^{\pm/0}$, which was compared with the prediction of DFT calculations in parallel with the case of H [74].

For the case of oxides, the donor-like Mu_D is in the diamagnetic state (Mu_D^+) in most cases, for which it is difficult to estimate ε_+ (< 0) by observing change in the valence state with elevating temperature (i.e., the ionization of Mu_D^0). In contrast, Mu_A is often observed in a paramagnetic state (Mu_A^0). Therefore, ε_- can be evaluated experimentally by observing the promotion of Mu_A^0 to Mu_A^- at sufficiently high temperatures ($kT \gg \varepsilon_-$). It is a future task to evaluate the pinning level $E^{+/-}$ by combining the information about ε_- and those for the Mu_D states, and to discuss what kind of regularity can be presumed for $E^{+/-}$ in oxides.

F. Implications to Mu/H in other ionic compounds

The model of the bistable relaxed-excited states for Mu (Mu_D and Mu_A) is useful for understanding electronic states of Mu in other materials that were previously thought to be isolated anomalies. In the following, we will discuss Mu/H in iron pyrite (FeS_2) and sodium alanate (NaAlH_4) as such examples, which can be important materials for green technologies (solar cells, hydrogen storages) aimed at

a decarbonized society. Some general remarks are also made on the oxides that have been the focus of μSR studies over decades from the viewpoint of strongly correlated electron systems.

1. FeS_2

Iron pyrite has long been attracting attention as a promising optoelectronic material due to its suitable indirect band gap ($E_g \simeq 0.95$ eV) and high absorption coefficient ($> 10^5$ cm^{-1} at $E_g \pm 0.1$ eV), which opens up great potential for emerging renewable energy applications, including photovoltaics, photodetectors, and photoelectrochemical cells. Until recently, the low open-circuit photovoltage ($V_{\text{oc}} \sim 0.2$ V) that comprises the main obstacle to these applications have been attributed to surface defect states. Regarding the heterogeneous bandgap and Fermi level pinning, sulfur vacancies has been a primary suspect. However, recent theoretical investigations suggest that this is not necessarily the case [123], leading to the renewed interest to the circumstantial evidence that H is involved in the n -type conductivity of unknown origin with activation energies less than 0.01 eV [124]. Moreover, electrochemical experiment suggests strikingly fast H diffusion in pyrite (corresponding diffusion coefficient $D_H \geq 2 \times 10^{-6}$ cm^2/s , comparable to that in bcc metals at ambient condition) [125, 126], which is further enhanced after saturation of defects by H [126].

Our recent muon study has serendipitously revealed that there are two different Mu states in pyrite, one is situated near the center of an Fe^{2+} -cornered tetrahedron with a nearly isotropic hyperfine parameter [Mu_p^0 , $A = 0.41(4)$ GHz], and the other as a diamagnetic state (Mu_d) located near the antibonding site of the S_2^{2-} dimer [127]. Their response to thermal agitation indicates that the Mu_d center accompanies the $E^{+/0}$ level within the conduction band, while the electronic structure of Mu_p^0 is more isolated from the host than Mu_d to form a deep in-gap level. The possibility of fast migration for Mu_p^0 to form a complex defect state with existing impurities at low temperatures ($T \leq 100$ K) and its fast diffusion at higher temperatures upon release from the complex ($T \geq 150$ K) has been suggested [127].

That the Mu_p^0 state is also present at higher temperatures is confirmed by our very recent additional muon Knight shift measurements. As shown in Fig. 8, Mu in pyrite has a component with a large positive shift that cannot be explained by chemical shifts associated with Mu_d , indicating that this is the signal from Mu_p^0 . Furthermore, the lack of the low-frequency side signal normally observed for Mu^0 is readily understood by considering that its electronic state is subject to a fast spin/charge exchange reaction with carriers [109] (as the sample is unintentionally n -type doped). The tendency of the shift to have a maximum around 300 K and a decrease at higher temperatures is also consistent with the expected Curie law dependence on temperature. The dashed curves in Fig. 8 are obtained by the least-square fit using a product of the Curie law and Arrhenius law, $K \propto (C/T) \exp(-E_a/kT)$

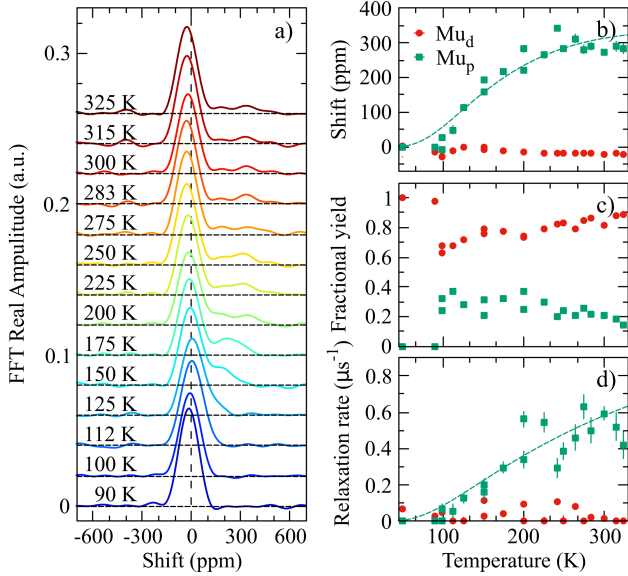


FIG. 8. Temperature dependence of the muon Knight shift observed in FeS_2 . a) Fast Fourier transform of the μSR spectra at typical temperatures measured under an external field of 6 T. The results of curve-fit analysis are shown for b) the frequency shift, c) fractional yields, and d) relaxation rate vs. temperature (T). For the dashed curves in b) and d), see text.

for b) with $E_a = 36(3)$ meV, and using the Arrhenius law, $\lambda \propto \exp(-E_p/kT)$ for d) with $E_p = 25$ meV (which are in reasonable agreement with the values estimated from the T dependence of the longitudinal depolarization rate [127]).

In retrospect, these two states can be readily understood as analogues of the donor/acceptor-like Mu states in oxides; Mu_d is assigned to the Mu_D forming a complex with S_2^{2-} anion whose electronic level falls in the conduction band to leave persistent Mu_D^+ state, and Mu_p is to the Mu_A forming a complex state with four Fe^{2+} cations (which was previously speculated as a deep donor-like state of unknown origin [127]). It is noteworthy that the latter also exhibits the characteristic fast diffusion, which is also shared by the case of H in pyrite. Such similarities/correspondences suggest that the behavior of Mu/H in other metal chalcogenides is also understood within the same framework discussed for oxides.

2. NaAlH_4

Sodium alanate belongs to a class of complex hydrides that has emerged as one of the most promising hydrogen storage materials in recent years. While these materials commonly have an advantage of high H weight percentage, they are generally characterized by extremely slow H cycling kinetics that has precluded applications. The drastic improvement on the kinetics in NaAlH_4 at moderate temperatures (~ 100 C $^\circ$) attained by transition metal doping (e.g. a few percent of Ti) [128] has triggered a surge of investigation for the microscopic mechanism of the enhancement by various local probes

including implanted Mu. Here, the muon study aims to mimic the behavior of interstitial H which is relevant for understanding the intermediate (non-equilibrium) states of the kinetic processes inside the compound during H intake/release.

The NaAlH_4 crystal consists of Na^+ cations and alanate (AlH_4^-) anions in the tetragonal structure (space group $I4_1/a$). It is inferred from DFT calculations that the band structure is that of an ionic insulator ($E_g \simeq 6.7$ eV), in which the valence band mainly consists of hydrogen s - p orbitals from alanate ions while the conduction band is dominated by those from Na^+ ions [129]. In our previous report, the implanted Mu exhibited two different states, where the μSR signal with spontaneous spin precessions characteristic of a three-spin system consisting of μ^+ -two proton nuclear spins was attributed to the AlH_4^- - Mu^+ - AlH_4^- complex, and the signal indicating Gaussian Kubo-Toyabe relaxation was attributed to an isolated Mu^+ at the octahedral interstitial position (O-site) [130]. By applying our model, we are now able to provide a more detailed discussion on the local electronic structure of these observed states.

From first-principles DFT calculations on the H-related native defects, the state corresponding to H_i^- is predicted to form the AlH_4^- - H^- - AlH_4^- complex, where H^- is stabilized by the bonding character with Al^{3+} . While for H_i^+ , it reacts with AlH_4^- to generate the H_2^+ molecule ($2\text{AlH}_4^- + \text{H}^+ \rightarrow \text{AlH}_3^- \cdot \text{AlH}_4^- + \text{H}_2^+$) [131–133]. It is tempting to consider that the state observed as a few-spin system may correspond to H_i^- . However, as shown in Fig. 9a, there are six proton nuclei on two nearest neighboring AlH_4^- 's equidistant from Mu that will lead to the Gaussian Kubo-Toyabe relaxation (the contribution of ^{23}Na nuclei is negligible). Thus, the state previously attributed to the isolated Mu^+ at the O site is interpreted to be the AlH_4^- - Mu^- - AlH_4^- complex, corresponding to M_A^- . In fact, the observed Gaussian relaxation rate ($\Delta = 0.4$ – 0.5 MHz) was significantly greater than that expected for the O site (0.33 MHz), suggesting the displacement of Mu towards AlH_4^- units [130].

The DFT calculations also suggest that the H_i^- ions can move with relatively small activation energy (0.16 eV) [133]. The muon study has also shown that the Mu_A^- -like state exhibits diffusion by hopping motion with a rate comparable with that observed for Mu^+ in fcc metals ($\sim 10^{-9}$ – 10^{-10} cm 2 /s at ambient temperature), and that its relative yield is significantly enhanced in place of the Mu_D^+ state by the Ti doping [130]. That the hopping rate of Mu_A^- is much smaller than that of Mu_A^0 (by 10^{-3} , see Fig. 6) may be attributed to the bonding character between the H $1s$ and Al sp^3 orbitals.

Regarding Mu_i^+ , when it forms a diatomic HMu^+ molecule by picking up a H atom (as in parallel with the case of native defects), it is expected to behave as a paramagnetic center (“muonated radical”, where muon spin is subject to a large hyperfine field from an unpaired electron). But no such paramagnetic Mu has been observed experimentally. Moreover, even if it forms a neutral HMu molecule (which would also exhibit spontaneous muon spin precession characteristic to two-spin systems), the distance between Mu and proton nuclear spin ($r = 0.074$ nm) is too small to account for the experimentally deduced value ($= 0.145$ nm; note that the spin precession

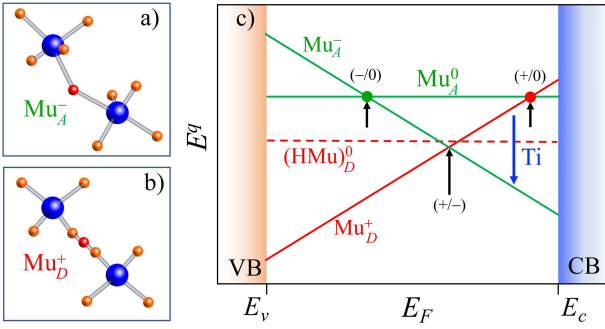


FIG. 9. The proposed models of a) Mu_A^- where a H^- atom bridging two AlH_4^- units in the $\text{AlH}_4^- - \text{H}^- - \text{AlH}_4^-$ complex [133] is replaced by Mu^- , and b) Mu_D^+ where a Mu^+ atom bridges two H atoms of AlH_4^- by the hydrogen bonding [130]. c) Schematic diagram showing the formation energy of Mu-related defects (E^q) vs. Fermi level (E_F) in NaAlH_4 . The initial Mu states correspond to those accompanying $E^{\pm/0}$ levels. The vertical arrow indicates the redox process catalyzed by Ti doping for $E_F > E^{+/-}$.

frequency is inversely proportional to r^3). The scarcity of the isolated interstitial H for Mu^+ to encounter in the ambient condition also disfavor the HMu molecular formation. Therefore, it is reasonable to assume that the observed signal is not from the HMu molecule (i.e., the thermodynamical ground state) but from the $\text{AlH}_4^- - \text{Mu}^+ - \text{AlH}_4^-$ complex (see Fig. 9b) [130], where the latter is realized as a metastable state (or stabilized by isotope effects due to the light mass of Mu).

The relationship between the formation energy and Fermi level of these states based on the results of DFT calculations is depicted in Fig. 9c [131, 133], where E^+ for Mu_A^+ is presumed to follow that of the H vacancy (V_{H}^+). From the viewpoint of the local electronic excitation [e.g., Eq.(3)], the absence of the Mu^0 state suggests that the $(\text{AlH}_3)^-$ state is not stable as an excited hole in the anion sublattice, and that the electronic excitation associated with muon implantation is dominated by the process $\text{AlH}_4^- + h\nu \rightarrow (\text{AlH}_3)^0 (= V_{\text{H}}^+) + \text{H}_i^-$. For Mu_D^+ , it is natural to assume the occurrence of the $\text{AlH}_4^- - \text{Mu}^+ - \text{AlH}_4^-$ complex as a metastable state. The relative yields of Mu_D^+ and Mu_A^- are consistent with the presumption that these states are generated with equal probabilities to satisfy the charge-neutrality condition.

Given the formation energy shown in Fig. 9, we are now more confident that the role of Ti is to convert the Mu_D^+ state to the mobile Mu_A^- state; $\text{Mu}_D^+ + 2e^- \rightarrow \text{Mu}_A^-$, which can be interpreted as a redox process catalyzed by Ti (indicated by the vertical arrow in Fig. 9). In the thermal equilibrium, it is likely that E_F increases by Ti doping (electron donation), which reduces E^- and promotes H_A^- formation against H_D^+ .

3. Other narrow-gap oxides

There is a massive body of μSR research on transition metal oxides exhibiting superconductivity and/or magnetism, where implanted Mu has been implicitly presumed as a bystander

Mater.	E_g (eV)	Mu	Refs.
La_2CuO_4	1.5–2	Mu^+	[134]
$\text{YBa}_2\text{Cu}_3\text{O}_6$	~ 1.5	Mu^+	[135]
LaMnO_3	~ 1.5	Mu^+	[136]
Ne_2CuO_4	1–1.5	Mu^+	[137]

TABLE III. The electronic state of Mu in cuprates and manganites, where the bandgap of the parent compounds are listed [138].

(bare μ^+) with minimal perturbations to the host in most cases. As shown in Table III for typical compounds, these materials often have a small band gap (1–2 eV) even in the insulating phase, for which Mu is observed in a diamagnetic state with the relative yield of nearly 100%. Their band structure aligned to the vacuum level is also shown in Fig. 5, where the bottom of conduction bands lies between -3 and -5 eV. These suggest a situation similar to Fig. 4d where the donor levels for Mu are in the conduction band to allow only for the Mu^+ state. Moreover, most of the muon studies for cuprates is concerned with their metallic phases attained by carrier doping, where implanted muons have virtually no chance of forming the Mu^0 state due to the electrostatic shielding of the positive charge by conduction electrons. Thus, it is concluded that the interpretation of μSR results in those compounds are virtually unaffected by the ambipolar property of Mu in most cases.

However, it should be remembered for insulating magnetic compounds that implanted Mu can attract an electron to form a polaronic state under certain conditions, which makes the interpretation of muon result complicated by affecting the local magnetic structure [104, 105].

V. CONCLUSION

In this paper, we have introduced a model that explain the behavior of Mu and H in insulating oxides in a coherent manner. For the Mu part, it is crucial to consider non-equilibrium effects for the construction of a viable model. This leads to the conclusion that the information obtained from Mu is not about the equilibrium charge-transition levels ($E^{+/-}$), but about the donor/acceptor levels ($E^{\pm/0}$). The conclusion has been supported by the consistency between the electronic states of Mu predicted by the position of $E^{\pm/0}$ levels in the band structure evaluated by first-principles DFT calculations for H and those experimentally observed in oxides. In addition, by establishing a model that allows such a systematic understanding, two findings have been inductively derived. The first is the suggestion that the Mu_D^+ -bound excitons are the origin of “shallow donor”-like Mu states in relatively narrow-gapped oxides ($\lesssim 5$ eV), as inferred from their STE-like electronic structure. This will bring about a major change of perspective in our understanding of the electronic structure of Mu. Second, it is revealed that the acceptor-like Mu^0 has a common property of fast diffusion in oxides. This would be qualitatively true for H as well, although there is a correction for isotope effects.

These findings indicate that, by integrating i) the experimental data on the $E^{\pm/0}$ levels obtained from the Mu studies,

ii) those on the $E^{+/-}$ levels in the thermal equilibrium of H, and iii) the first-principles calculations based on the DFT theory, a coherent understanding on the behavior of hydrogen in materials can be achieved. The model will be also useful for clarifying the role of hydrogen in a wide range of non-metallic materials.

ACKNOWLEDGMENTS

The works of the authors quoted in this paper were conducted in collaboration with many colleagues. We would like to appreciate helpful discussions with K. Asakura, K. Fukutani, K. Ide, S. Iimura, T. U. Ito, W. Higemoto, Y. Kamiya, R. F. Kiefl, K. M. Kojima, R. L. Lichti, W. A. MacFarlane, S. Matsuishi, H. Miwa, F. Oba, N. Ohashi, T. Ohsawa, T. Prokschar, J. Robertson, M. Saito, K. Shimomura, A. L. Shluger, A. Suter, S. Tsuneyuki, and R. Vilão. This work was supported by the MEXT Elements Strategy Initiative to Form Core Research Center for Electron Materials (Grant No. JPMXP0112101001) and JSPS KAKENHI (Grant Nos. 19K15033 and 17H06153).

APPENDIX A: μ SR SPECTRUM WITHOUT UNPAIRED ELECTRONS

In the following, we summarize the typical cases of the hyperfine interactions between muon and nuclear/electron spins that is represented by the effective local magnetic field $\mathbf{H}(\mathbf{r})$ and the corresponding time variation of the muon spin polarization (time spectrum) to be observed.

Let us first consider non-magnetic materials where there are no unpaired electrons (correspond to Fig. 3b, f, h, and i). In these cases, the origin of $\mathbf{H}(\mathbf{r})$ is none other than the nuclear magnetic moments of the host. In general, the term "hyperfine interaction" includes both magnetic dipole interaction and the Fermi contact interaction. However, since both nuclei and muons are well localized in the ground state, the interaction between them is mainly magnetic dipole interaction. The Hamiltonian is then given as

$$\mathcal{H}/\hbar = \mathcal{H}_Z/\hbar + \mathcal{H}_d/\hbar, \quad (7)$$

$$\mathcal{H}_d/\hbar = \gamma_\mu \gamma_I \mathbf{S}_\mu \sum_i \hat{A}_d^i \mathbf{I}_i, \quad (8)$$

where \mathcal{H}_Z represents the Zeeman interaction for muon and nuclear spins, \mathbf{S}_μ is the muon spin, $\gamma_\mu = 2\pi \times 135.53$ MHz/T is the gyromagnetic ratio of muon spin, \mathbf{I}_i is the nuclear spin at distance r_i on the i th lattice point, γ_I is the gyromagnetic ratio of the nuclear spin, and \hat{A}_d^i is the magnetic dipole tensor

$$(\hat{A}_d^i)^{\alpha\beta} = \frac{1}{r_i^3} \left(\frac{3\alpha_i\beta_i}{r_i^2} - \delta_{\alpha\beta} \right) \quad (\alpha, \beta = x, y, z), \quad (9)$$

representing the hyperfine interaction between muon-nuclear magnetic moments. In the case of zero-external field ($\mathcal{H}_Z = 0$), the effective magnetic field expressed as

$$\mathbf{H}(\mathbf{r}) = \mathbf{H}_d = \gamma \sum_i \hat{A}_d^i \bar{\mathbf{I}}_i \quad (10)$$

is used to obtain the effective Hamiltonian

$$\mathcal{H}/\hbar = \gamma_\mu \mathbf{S}_\mu \cdot \mathbf{H}_d, \quad (11)$$

and the time evolution of the muon spin polarization $\mathbf{P}(t) = \langle \mathbf{S}_\mu(0) \cdot \mathbf{S}_\mu(t) \rangle / |\mathbf{S}_\mu|^2$ can be obtained analytically using the density matrix of the muon-nucleus spin system for a small number of nucleons (where $\gamma_I \bar{\mathbf{I}}_i$ is the effective magnetic moment considering the electric quadrupole interaction for $I_i \geq 1$).

On the other hand, if the coordination of the nuclear magnetic moment viewed from the muon is isotropic and the number of coordination is sufficiently large (≥ 4), the classical spin treatment is easier, and the density distribution $n(\mathbf{H})$ of $\mathbf{H}(\mathbf{r})$ is approximated by a Gaussian distribution with zero mean value,

$$n(H_\alpha) = \langle \delta(H_\alpha - H_\alpha(\mathbf{r})) \rangle_r = \frac{\gamma_\mu}{\sqrt{2\pi\Delta}} \exp\left(-\frac{\gamma_\mu^2 H_\alpha^2}{2\Delta^2}\right) \quad (\alpha = x, y, z) \quad (12)$$

Here, Δ is given by the second moment of \mathbf{H}_d as

$$\frac{\Delta^2}{\gamma_\mu^2} = \sum_i \sum_{\alpha, \beta} [\gamma_I (\hat{A}_d^i)^{\alpha\beta} \bar{\mathbf{I}}_i]^2, \quad (13)$$

with β taking all x, y, z , and the α over the x, y components that are effective for longitudinal relaxation when \hat{z} is the longitudinal direction; the z component does not contribute to the relaxation because it gives a magnetic field parallel to the muon spin. In this case, the spin polarization $\mathbf{G}(t)$ is given by the motion of one muon spin projected onto \mathbf{H} with the angle between the magnetic field \mathbf{H} and the \hat{z} axis as θ ,

$$P_z(t) = \cos^2 \theta + \sin^2 \theta \cos(\gamma_\mu H t) \quad (14)$$

which is averaged by $n(\mathbf{H})$ in Eq. (12) to yield the Kubo-Toyabe function

$$G_z(t) = \int \int \int_{-\infty}^{\infty} P_z(t) \Pi_{\alpha n \alpha}(H_\alpha) dH_\alpha = \frac{1}{3} + \frac{2}{3} (1 - \Delta^2 t^2) e^{-\frac{1}{2} \Delta^2 t^2}. \quad (15)$$

The magnitude of Δ is sensitive to the size of the nearest-neighbor nuclear magnetic moment $\gamma_I \bar{\mathbf{I}}_i$ and the distance r_i from the muon, and the position occupied by the muon as pseudo-hydrogen can be estimated by comparing the experimentally obtained Δ with the calculated value at the candidate sites. Especially in recent years, the reliability of the first-principles calculations based on density functional theory (DFT) have been improved, and by using this method to narrow down the candidate sites, the muon sites can be estimated with higher credibility.

APPENDIX B: μ SR SPECTRUM IN THE PRESENCE OF UNPAIRED ELECTRONS

As in the previous section, the host is assumed to be a non-magnetic material. In this case, the unpaired electron originates from that bound to the muon (Mu^0) (corresponding to Fig. 3c, d, e, and g). In general, the Hamiltonian for the magnetic interaction between muon and unpaired electron is given by

$$\mathcal{H}/\hbar = [\mathcal{H}_d + \mathcal{H}_e + \mathcal{H}_{\text{Mu}}]/\hbar, \quad (16)$$

$$\mathcal{H}_{\text{Mu}}/\hbar = \gamma_\mu \gamma_e S_e \left[\frac{8\pi}{3} \delta(r) + \hat{A}_d \right] S_\mu \quad (17)$$

$$= \frac{1}{2} (2\pi A) \cdot S_\mu = \frac{1}{2} \omega_{\text{Mu}} \cdot S_\mu, \quad (18)$$

where \mathcal{H}_d is the muon-nuclear spin system [Eq. (8)], and \mathcal{H}_e is the Hamiltonian of the electron system with γ_e being the gyromagnetic ratio of the electron ($= 2\pi \times 28.02421$ GHz/T). The first term in \mathcal{H}_{Mu} is for the Fermi contact interaction, and the second term is for the magnetic dipolar interaction.

Provided that the magnitudes of interactions between nuclear spins and muons/electrons are negligible, Eq. (16) is a two-spin Hamiltonian whose eigenstates are given by the linear combination of the muon electron spin eigenfunctions $|s_z^\mu, s_z^e\rangle$ ($s_z^\mu, s_z^e = \pm 1/2$), with four corresponding eigenenergies ($E_m, m = 1-4$). When an external magnetic field \mathbf{H}_0 is applied, the spin rotation signals corresponding to the allowed transitions between these eigenstates,

$$G(t) = \sum_{n < m} a_{nm} \cos \omega_{nm} t, \quad (19)$$

are observed, where $\omega_{nm} = \omega_n - \omega_m = (E_n - E_m)/\hbar$ are the spin rotation frequencies and a_{nm} are their amplitudes.

Now, taking \hat{z} as the main axis of the hyperfine interaction ω_{Mu} with θ and ϕ being the polar and the azimuthal angles, Eq. (18) is expressed as

$$\begin{aligned} \mathcal{H}_{\text{Mu}}/\hbar &= \frac{1}{2} \omega_{\text{Mu}}(\theta, \phi) = \frac{1}{2} 2\pi A(\theta, \phi), \\ A(\theta, \phi) &= (A_x \cos^2 \phi + A_y \sin^2 \phi) \sin^2 \theta \\ &\quad + A_z \cos^2 \theta, \end{aligned} \quad (20)$$

with which we can sort out the qualitative relationship between the electronic structure of Mu^0 with surrounding atoms and that of $A(\theta, \phi)$.

The reason for the formation of bound states is the relatively weak local dielectric shielding (determined by the permittivity ϵ) that leads to the long-range Coulomb interaction between muons and electrons. If the bound electron is in a 1s orbital-like state (as shown in Fig. 3c), the hyperfine interaction is dominated by the Fermi contact term and is isotropic with positive sign as a whole ($A_x \simeq A_y \simeq A_z > 0$). In this case, the absolute value of A , the effective Bohr radius, and

the depth of the bound level are estimated to be

$$A \simeq \frac{\omega_{\text{vac}}}{2\pi} \left[\frac{m^*}{\epsilon' m_e} \right]^3, \quad (21)$$

$$a^* \simeq a_0 \frac{\epsilon' m^*}{m_e}, \quad (22)$$

$$R^* \simeq R_y \frac{m^*}{\epsilon'^2 m_e}, \quad (23)$$

where m^* is the effective mass of the electron in the conduction band, R_y is Rydberg's constant, and ϵ' is the relative permittivity at zero frequency [$= \epsilon(\omega \rightarrow 0)/\epsilon$]. This is thought to be one of the mechanisms by which shallow donor levels are induced by interstitial hydrogen in semiconductors with high permittivity.

However, such a Jellium model is not sufficient for actual materials, and the electronic states of H/Mu are anisotropically distributed due to interactions with surrounding atoms. One such example is Mu^0 located near the bonding center between host atoms, which has been known for a long time in elemental semiconductors with diamond structure and in group 13-15 compound semiconductors such as GaAs with zinc blende structure (corresponding to Mu_D in Fig. 1b) [38]. In these examples, the hosts have a four-coordinate configuration with sp^3 hybrid orbitals that are strongly covalent, and Mu/H breaks this bond to make a new bond with the anion (I^-), and the excess electrons become a dangling bond on the cation (K^+) (see Fig. 1c,d). In this case, the hyperfine interaction has an anisotropy symmetric around the axis connecting the muon and the electron, and by taking the symmetry axis to \hat{z} , Eq. (20) is reduced to

$$A(\theta, \phi) = A^* + D \cos^2 \theta \quad (24)$$

with $A_{x,y} \equiv A_\perp \equiv A^* - D/2$ and $A_z \equiv A_\parallel \equiv A^* + D$. The first reported Mu^0 with shallow electronic levels were found in II-VI compounds such as zinc oxide (ZnO) [53, 54], which also exhibits hyperfine interactions well described by Eq. (24).

APPENDIX C: A MODEL FOR THE H/MU SITE OCCUPANCY OF THE ASYMMETRIC DOUBLE-WELL POTENTIAL

We consider a simple model for the temperature dependence of the H/Mu site occupancy in the presence of two sites (Site-A and -D, see Fig. 2a) with asymmetric double-well potential separated by a potential barrier (V and V'). Provided that $V' \gg V$, the partition function for the two-level system is approximately given by

$$Z(\beta) = n_D + n_A e^{-\beta V}, \quad (25)$$

where $\beta \equiv 1/k_B T$, n_A and n_D are the degeneracy of the each site in the unit cell. The fractional occupancy of Mu/H for the respective sites in the equilibrium state is then described by

$$f_A = \frac{n_A e^{-\beta V}}{n_D + n_A e^{-\beta V}}, \quad (26)$$

$$f_D = \frac{n_D}{n_D + n_A e^{-\beta V}}. \quad (27)$$

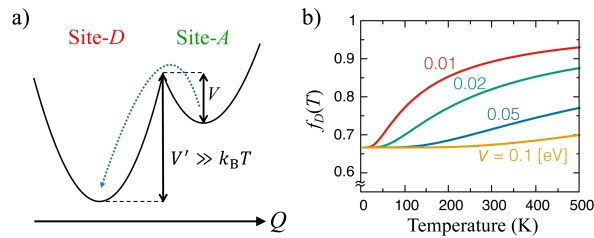


FIG. 10. (a): Schematic drawing of the two-site model based on the Boltzmann factor. (b): Temperature dependence of Eq. (28) for various V with $f_D^0 = 2/3$, $f_A^0 = 1/3$.

Note that $f_D < 1$ at finite temperatures ($n_A e^{-\beta V} > 0$) to reduce the free energy by gaining entropy.

Now, we presume that the initial site occupancy for Mu is that quenched from $T = \infty$ ($\beta = 0$), so that $f_A = n_A/(n_A + n_D) \equiv f_A^0$, $f_D = n_D/(n_A + n_D) \equiv f_D^0$ (i.e., proportional to the number density of available sites). Then, the fractional yields observed by μ SR at the finite temperature correspond to the average fraction of muons over the annealing process from this initial distribution to the thermal equilibrium distribution

(Eqs. 26, 27) in the time scale of $\sim 10^1 \mu$ s. Such a relaxation process is generally described by the fluctuation-dissipation theorem within the linear response theory for the macroscopic systems.

However, since the implanted Mu as microscopic entity probes the local fluctuations only, we assume that the observed temperature dependence of f_D is determined by the migration from Site-A to Site-D via thermally activated hopping over a potential barrier V [see Fig. 10 (a)], where the migration probability is proportional to $e^{-\beta V}$. The observed fraction of muons at Site-A can be approximately given by $f_A(T) \simeq f_A^0 (1 - e^{-\beta V})$, which is valid for low temperatures ($V' \gg k_B T$) where the inverse hopping process is negligible. Thus have

$$f_D(T) = 1 - f_A(T) \simeq f_D^0 + f_A^0 e^{-\beta V}, \quad (28)$$

for the temperature dependence of the Mu occupancy at Site-D. Fig. 10 (b) shows examples of $f_D(T)$ given by Eq. (28) for various V .

-
- [1] J. Pankove and N. M. Johnson, *Hydrogen in Semiconductors* (Academic, New York, 1991).
- [2] S. J. Pearton, J. W. Corbett, and M. Stavola, *Hydrogen in Crystalline Semiconductors* (Springer, Berlin, 1992).
- [3] See, for example, A. Yaouanc, and P. D. de Réotier, *Muon Spin Rotation, Relaxation, and Resonance* (Oxford Univ. Press, 2011).
- [4] M. Hiraishi, K. M. Kojima, M. Miyazaki, I. Yamauchi, H. Okabe, A. Koda, R. Kadono, S. Matsuishi, and H. Hosono, “Cage electron-hydroxyl complex state as electron donor in mayenite,” *Phys. Rev. B* **93**, 121201 (2016).
- [5] T. Prokscha, E. Morenzoni, D. G. Eshchenko, N. Garifianov, H. Glückler, R. Khasanov, H. Luetkens, and A. Suter, “Formation of hydrogen impurity states in silicon and insulators at low implantation energies,” *Phys. Rev. Lett.* **98**, 227401 (2007).
- [6] C. G. Van de Walle and J. Neugebauer, “First-principles calculations for defects and impurities: Applications to III-nitrides,” *J. Appl. Phys.* **95**, 3851–3879 (2004).
- [7] P. W. Anderson, “Model for the electronic structure of amorphous semiconductors,” *Phys. Rev. Lett.* **34**, 953–955 (1975).
- [8] J. Neugebauer and C. G. Van de Walle, “Hydrogen in GaN: Novel aspects of a common impurity,” *Phys. Rev. Lett.* **75**, 4452–4455 (1995).
- [9] A. Yokozawa and Y. Miyamoto, “First-principles calculations for charged states of hydrogen atoms in SiO₂,” *Phys. Rev. B* **55**, 13783–13788 (1997).
- [10] S. Lany and A. Zunger, “Assessment of correction methods for the band-gap problem and for finite-size effects in supercell defect calculations: Case studies for ZnO and GaAs,” *Phys. Rev. B* **78**, 235104 (2008).
- [11] H. Li and J. Robertson, “Behaviour of hydrogen in wide band gap oxides,” *J. Appl. Phys.* **115**, 203708 (2014).
- [12] M. D. Segall, P. J. D. Lindan, M. J. Probert, C. J. Pickard, P. J. Hasnip, S. J. Clark, and M. C. Payne, “First-principles simulation: ideas, illustrations and the CASTEP code,” *J. Phys.: Condens. Matt.* **14**, 2717–2744 (2002).
- [13] J. Heyd, G. E. Scuseria, and M. Ernzerhof, “Hybrid functionals based on a screened coulomb potential,” *J. Chem. Phys.* **118**, 8207–8215 (2003).
- [14] J. Heyd, G. E. Scuseria, and M. Ernzerhof, “Erratum: “hybrid functionals based on a screened coulomb potential” [J. Chem. Phys. **118**, 8207 (2003)],” *J. Chem. Phys.* **124**, 219906 (2006).
- [15] F. Kerkhoff, W. Martienssen, and W. Sander, “Elektronenspin-resonanz und photochemie des U₂-zentrums in alkalihalogenid-kristallen,” *Z. Phys.* **173**, 184–202 (1963).
- [16] J. M. Spaeth and M. Sturm, “ESR and ENDOR investigation of interstitial hydrogen atoms in alkali halides,” *Phys. Stat. Sol. (b)* **42**, 739–748 (1970).
- [17] S. P. Morato and F. Lüty, “Hydrogen defects from uv photodissociation of OH⁻ centers in alkali halides,” *Phys. Rev. B* **22**, 4980–4991 (1980).
- [18] See, for example, K. S. Song, and R. T. Williams, *Self-Trapped Excitons* (Springer, Berlin, 1996).
- [19] N. Itoh, “Bond scission induced by electronic excitation in solids: A tool for nanomanipulation,” *Nucl. Instr. Meth. Phys. Res. B* **122**, 405–409 (1997).
- [20] K. Cho, H. Kamimura, and Y. Uemura, “Electronic structures of the U₂-center in KCl and KBr: II –the effect of the configuration mixing–,” *J. Phys. Soc. Jpn.* **21**, 2244–2252 (1966).
- [21] Hp. Baumeler, R. F. Kiefl, H. Keller, W. Kündig, W. Odermatt, B. D. Patterson, J. W. Schneider, T. L. Estle, S. P. Rudaz, D. P. Spencer, K. W. Blazey, and I. M. Savić, “Muonium centers in the alkali halides,” *Hyperfine Interact.* **32**, 659–665 (1986).
- [22] T. E. Tsai, D. L. Griscom, and E. J. Friebele, “Medium-range structural order and fractal annealing kinetics of radiolytic atomic hydrogen in high-purity silica,” *Phys. Rev. B* **40**, 6374–6380 (1989).
- [23] L. Verdi and A. Miotello, “Hydrogen dimerization process: A probe for investigation of the α -SiO₂ structure,” *Phys. Rev. B* **47**, 14187–14192 (1993).

- [24] T. Ichikawa and V. Kurshev, "Spin-lattice relaxation of the hydrogen atom in a fused quartz," *J. Chem. Phys.* **99**, 5728–5735 (1993).
- [25] I. A. Shkrob and A. D. Trifunac, "Time-resolved EPR of spin-polarized mobile H atoms in amorphous silica: The involvement of small polarons," *Phys. Rev. B* **54**, 15073–15078 (1996).
- [26] I. A. Shkrob and A. D. Trifunac, "Spin-polarized H/D atoms and radiation chemistry in amorphous silica," *J. Chem. Phys.* **107**, 2374–2385 (1997).
- [27] I. A. Shkrob, B. M. Tadjikov, S. D. Chemerisov, and A. D. Trifunac, "Electron trapping and hydrogen atoms in oxide glasses," *J. Chem. Phys.* **111**, 5124–5140 (1999).
- [28] D. Muñoz Ramo, P. V. Sushko, and A. L. Shluger, "Models of triplet self-trapped excitons in SiO₂, HfO₂, and HfSiO₄," *Phys. Rev. B* **85**, 024120 (2012).
- [29] A.-M. El-Sayed, Y. Wimmer, W. Goes, T. Grasser, V. V. Afanas'ev, and A. L. Shluger, "Theoretical models of hydrogen-induced defects in amorphous silicon dioxide," *Phys. Rev. B* **92**, 014107 (2015).
- [30] See, for example, P. Y. Yu, and M. Cardona, *Fundamentals of Semiconductors – Physics and Materials Properties* (Springer Berlin Heidelberg New York, 2005).
- [31] R. Kadono, A. Matsushita, and K. Nagamine, "Muonium fluorescence: Anomalous muonium center and relaxed excited state in KBr," *Phys. Rev. Lett.* **67**, 3689–3691 (1991).
- [32] R. Kadono, A. Matsushita, K. Nishiyama, and K. Nagamine, "Muon-induced luminescence in KBr," *Phys. Rev. B* **46**, 8586–8588 (1992).
- [33] V. Storchak, S. F. J. Cox, S. P. Cottrell, J. H. Brewer, G. D. Morris, D. J. Arseneau, and B. Hitti, "Muonium formation via electron transport in silicon," *Phys. Rev. Lett.* **78**, 2835–2838 (1997).
- [34] D. G. Eshchenko, V. G. Storchak, and G. D. Morris, "Electron transport to positive centers in GaAs," *Physics Letters A* **264**, 226–231 (1999).
- [35] D. G. Eshchenko, V. G. Storchak, S. P. Cottrell, and S. F. J. Cox, "Excited muonium state in CdS," *Phys. Rev. B* **68**, 073201 (2003).
- [36] G. A. Jeffery, *An Introduction to Hydrogen Bonding* (Oxford University Press, New York, 1997).
- [37] J. H. Brewer, S. R. Kreitzman, D. R. Noakes, E. J. Ansaldo, D. R. Harshman, and R. Keitel, "Observation of muon-fluorine "hydrogen bonding" in ionic crystals," *Phys. Rev. B* **33**, 7813–7816 (1986).
- [38] B. D. Patterson, "Muonium states in semiconductors," *Rev. Mod. Phys.* **60**, 69–159 (1988).
- [39] R. C. Vilão, R. B. L. Vieira, H. V. Alberto, J. M. Gil, A. Weidinger, R. L. Lichti, P. W. Mengyan, B. B. Baker, and J. S. Lord, "Barrier model in muon implantation and application to Lu₂O₃," *Phys. Rev. B* **98**, 115201 (2018).
- [40] R. C. Vilão, H. V. Alberto, J. M. Gil, and A. Weidinger, "Thermal spike in muon implantation," *Phys. Rev. B* **99**, 195206 (2019).
- [41] M. Toulemonde, J.M. Costantini, Ch. Dufour, A. Meftah, E. Paumier, and F. Studer, "Track creation in SiO₂ and BaFe₁₂O₁₉ by swift heavy ions: a thermal spike description," *Nucl. Inst. Meth. Phys. Res. Sec. B* **116**, 37–42 (1996), radiation Effects in Insulators.
- [42] R. C. Vilão, R. B. L. Vieira, H. V. Alberto, J. M. Gil, and A. Weidinger, "Role of the transition state in muon implantation," *Phys. Rev. B* **96**, 195205 (2017).
- [43] G. G. Myasishcheva, Yu. V. Obukhov, V. S. Roganov, and V. G. Firsov, "A search for atomic muonium in chemically inert substances," *Sov. Phys. JETP* **26**, 298–301 (1968).
- [44] D. P. Spencer, D. G. Fleming, and J. H. Brewer, "Muonium formation in diamond and oxide insulators," *Hyperfine Interact.* **18**, 567–573 (1984).
- [45] E. V. Minaichev, G. G. Myasishcheva, Yu. V. Obukhov, V. S. Roganov, G. I. Savel'ev, and V. G. Firsov, "Paschen-Back effect for the muonium atom," *Sov. Phys. JETP* **31**, 849–852 (1970).
- [46] R. F. Kiefl, W. Odermatt, Hp. Baumeler, J. Felber, H. Keller, W. Kündig, P. F. Meier, B. D. Patterson, J. W. Schneider, K. W. Blazey, T. L. Estle, and C. Schwab, "Muonium centers in the cuprous halides," *Phys. Rev. B* **34**, 1474–1484 (1986).
- [47] S. F. J. Cox, J. L. Gavartin, J. S. Lord, S. P. Cottrell, J. M. Gil, H. V. Alberto, J. Pirotto Duarte, R. C. Vilão, N. Ayres de Campos, D. J. Keeble, E. A. Davis, M Charlton, and D. P. van der Werf, "Oxide muonics: II. modelling the electrical activity of hydrogen in wide-gap and high-permittivity dielectrics," *J. Phys.: Condens. Matt.* **18**, 1079–1119 (2006).
- [48] A. G. Marinopoulos, R. C. Vilão, R. B. L. Vieira, H. V. Alberto, J. M. Gil, M. V. Yakushev, R. Scheuermann, and T. Goko, "Defect levels and hyperfine constants of hydrogen in beryllium oxide from hybrid-functional calculations and muonium spectroscopy," *Phil. Mag.* **97**, 2108–2128 (2017).
- [49] R. B. L. Vieira, R. C. Vilão, H. V. Alberto, J. M. Gil, A. Weidinger, B. B. Baker, P. W. Mengyan, and R. L. Lichti, "High-field study of muonium states in HfO₂ and ZrO₂," *J. Phys.: Conf. Ser.* **551**, 012048 (2014).
- [50] R. B. L. Vieira, R. C. Vilão, A. G. Marinopoulos, P. M. Gordo, J. A. Paixão, H. V. Alberto, J. M. Gil, A. Weidinger, R. L. Lichti, B. Baker, P. W. Mengyan, and J. S. Lord, "Isolated hydrogen configurations in zirconia as seen by muon spin spectroscopy and ab initio calculations," *Phys. Rev. B* **94**, 115207 (2016).
- [51] E. L. Silva, A. G. Marinopoulos, R. C. Vilão, R. B. L. Vieira, H. V. Alberto, J. Pirotto Duarte, and J. M. Gil, "Hydrogen impurity in yttria: Ab initio and μ SR perspectives," *Phys. Rev. B* **85**, 165211 (2012).
- [52] E. Lora da Silva, A. G. Marinopoulos, R. B. L. Vieira, R. C. Vilão, H. V. Alberto, J. M. Gil, R. L. Lichti, P. W. Mengyan, and B. B. Baker, "Electronic structure of interstitial hydrogen in lutetium oxide from DFT + U calculations and comparison study with μ SR spectroscopy," *Phys. Rev. B* **94**, 014104 (2016).
- [53] S. F. J. Cox, E. A. Davis, S. P. Cottrell, P. J. C. King, J. S. Lord, J. M. Gil, H. V. Alberto, R. C. Vilão, J. Pirotto Duarte, N. Ayres de Campos, A. Weidinger, R. L. Lichti, and S. J. C. Irvine, "Experimental confirmation of the predicted shallow donor hydrogen state in zinc oxide," *Phys. Rev. Lett.* **86**, 2601–2604 (2001).
- [54] K. Shimomura, K. Nishiyama, and R. Kadono, "Electronic structure of the muonium center as a shallow donor in ZnO," *Phys. Rev. Lett.* **89**, 255505 (2002).
- [55] C. G. Van de Walle, "Hydrogen as a cause of doping in zinc oxide," *Phys. Rev. Lett.* **85**, 1012–1015 (2000).
- [56] K. Shimomura, R. Kadono, A. Koda, K. Nishiyama, and M. Mihara, "Electronic structure of Mu-complex donor state in rutile TiO₂," *Phys. Rev. B* **92**, 075203 (2015).
- [57] R. C. Vilão, R. B. L. Vieira, H. V. Alberto, J. M. Gil, A. Weidinger, R. L. Lichti, B. B. Baker, P. W. Mengyan, and J. S. Lord, "Muonium donor in rutile TiO₂ and comparison with hydrogen," *Phys. Rev. B* **92**, 081202 (2015).
- [58] A. T. Brant, Shan Yang, N. C. Giles, and L. E. Halliburton, "Hydrogen donors and Ti³⁺ ions in reduced TiO₂ crystals," *J. Appl. Phys.* **110**, 053714 (2011).

- [59] T. U. Ito, W. Higemoto, A. Koda, and K. Shimomura, "Polaronic nature of a muonium-related paramagnetic center in SrTiO₃," *Appl. Phys. Lett.* **115**, 192103 (2019).
- [60] Y. Iwazaki, T. Suzuki, and S. Tsuneyuki, "Negatively charged hydrogen at oxygen-vacancy sites in BaTiO₃: Density-functional calculation," *J. Appl. Phys.* **108**, 083705 (2010).
- [61] S. Iimura, S. Matsuishi, H. Sato, T. Hanna, Y. Muraba, S. W. Kim, J. E. Kim, M. Takata, and H. Hosono, "Two-dome structure in electron-doped iron arsenide superconductors," *Nature Comm.* **3**, 943 (2012).
- [62] K. M. Kojima, M. Hiraishi, H. Okabe, A. Koda, R. Kadono, K. Ide, S. Matsuishi, H. Kumomi, T. Kamiya, and H. Hosono, "Electronic structure of interstitial hydrogen in In-Ga-Zn-O semiconductor simulated by muon," *Appl. Phys. Lett.* **115**, 122104 (2019).
- [63] H. Li, Y. Guo, and J. Robertson, "Oxygen vacancies and hydrogen in amorphous In-Ga-Zn-O and ZnO," *Phys. Rev. Materials* **2**, 074601 (2018).
- [64] K. Nomura, T. Kamiya, H. Yanagi, E. Ikenaga, K. Yang, K. Kobayashi, M. Hirano, and H. Hosono, "Subgap states in transparent amorphous oxide semiconductor, In-Ga-Zn-O, observed by bulk sensitive x-ray photoelectron spectroscopy," *Appl. Phys. Lett.* **92**, 202117 (2008).
- [65] K. Nomura, T. Kamiya, E. Ikenaga, H. Yanagi, K. Kobayashi, and H. Hosono, "Depth analysis of subgap electronic states in amorphous oxide semiconductor, a-In-Ga-Zn-O, studied by hard x-ray photoelectron spectroscopy," *J. Appl. Phys.* **109**, 073726 (2011).
- [66] J. K. Jeong, "Photo-bias instability of metal oxide thin film transistors for advanced active matrix displays," *J. Mater. Res.* **28**, 2071–2084 (2013).
- [67] T. U. Ito, A. Koda, K. Shimomura, W. Higemoto, T. Matsuzaki, Y. Kobayashi, and H. Kageyama, "Excited configurations of hydrogen in the BaTiO_{3-x}H_x perovskite lattice associated with hydrogen exchange and transport," *Phys. Rev. B* **95**, 020301 (2017).
- [68] Y. Iwazaki, Y. Gohda, and S. Tsuneyuki, "Diversity of hydrogen configuration and its roles in SrTiO_{3-δ}," *APL Mater.* **2**, 012103 (2014).
- [69] P. Ruetschi, "Cation-vacancy model for MnO₂," *J. Electrochem. Soc.* **131**, 2737–2744 (1984).
- [70] P. Ruetschi and R. Giovanoli, "Cation vacancies in MnO₂ and their influence on electrochemical reactivity," *J. Electrochem. Soc.* **135**, 2663–2669 (1988).
- [71] H. Okabe, M. Hiraishi, A. Koda, S. Takeshita, K. M. Kojima, I. Yamauchi, T. Ohsawa, N. Ohashi, H. Sato, and R. Kadono, "Local electronic structure of dilute hydrogen in β-MnO₂," *Phys. Rev. B* **103**, 155121 (2021).
- [72] Ç. Kılıç and A. Zunger, "n-type doping of oxides by hydrogen," *Appl. Phys. Lett.* **81**, 73–75 (2002).
- [73] S. F. J. Cox, J. S. Lord, S. P. Cottrell, J. M. Gil, H. V. Alberto, A. Keren, D. Prabhakaran, R. Scheuermann, and A. Stoykov, "Oxide muonics: I. modelling the electrical activity of hydrogen in semiconducting oxides," *J. Phys.: Condens. Matt.* **18**, 1061–1078 (2006).
- [74] R. L. Lichti, K. H. Chow, and S. F. J. Cox, "Hydrogen defect-level pinning in semiconductors: The muonium equivalent," *Phys. Rev. Lett.* **101**, 136403 (2008).
- [75] C. G. Van de Walle and J. Neugebauer, "Universal alignment of hydrogen levels in semiconductors, insulators and solutions," *Nature* **423**, 626–628 (2003).
- [76] R. F. Kiefl, E. Holzschuh, H. Keller, W. Kündig, P. F. Meier, B. D. Patterson, J. W. Schneider, K. W. Blazey, S. L. Rudaz, and A. B. Denison, "Decoupling of muonium in high transverse magnetic fields," *Phys. Rev. Lett.* **53**, 90–93 (1984).
- [77] A. G. Marinopoulos, "Incorporation and migration of hydrogen in yttria-stabilized cubic zirconia: Insights from semilocal and hybrid-functional calculations," *Phys. Rev. B* **86**, 155144 (2012).
- [78] P. D. C. King, I. McKenzie, and T. D. Veal, "Observation of shallow-donor muonium in Ga₂O₃: Evidence for hydrogen-induced conductivity," *Appl. Phys. Lett.* **96**, 062110 (2010).
- [79] P. D. C. King, R. L. Lichti, Y. G. Celebi, J. M. Gil, R. C. Vilão, H. V. Alberto, J. Piroto Duarte, D. J. Payne, R. G. Egdell, I. McKenzie, C. F. McConville, S. F. J. Cox, and T. D. Veal, "Shallow donor state of hydrogen in In₂O₃ and SnO₂: Implications for conductivity in transparent conducting oxides," *Phys. Rev. B* **80**, 081201 (2009).
- [80] F. Oba, A. Togo, I. Tanaka, J. Paier, and G. Kresse, "Defect energetics in ZnO: A hybrid hartree-fock density functional study," *Phys. Rev. B* **77**, 245202 (2008).
- [81] R. C. Vilão, A. G. Marinopoulos, R. B. L. Vieira, A. Weidinger, H. V. Alberto, J. Piroto Duarte, J. M. Gil, J. S. Lord, and S. F. J. Cox, "Hydrogen impurity in paratellurite α-TeO₂: Muon-spin rotation and ab initio studies," *Phys. Rev. B* **84**, 045201 (2011).
- [82] Z. Salman, T. Prokscha, A. Amato, E. Morenzoni, R. Scheuermann, K. Sedlak, and A. Suter, "Direct spectroscopic observation of a shallow hydrogenlike donor state in insulating SrTiO₃," *Phys. Rev. Lett.* **113**, 156801 (2014).
- [83] J. B. Varley, A. Janotti, and C. G. Van de Walle, "Hydrogenated vacancies and hidden hydrogen in SrTiO₃," *Phys. Rev. B* **89**, 075202 (2014).
- [84] S. Limpijumngong, P. Reunchan, A. Janotti, and C. G. Van de Walle, "Hydrogen doping in indium oxide: An ab initio study," *Phys. Rev. B* **80**, 193202 (2009).
- [85] K. Shimomura, R. Kadono, K. Ohishi, M. Mizuta, M. Saito, K. H. Chow, B. Hitti, and R. L. Lichti, "Muonium as a shallow center in GaN," *Phys. Rev. Lett.* **92**, 135505 (2004).
- [86] S. Limpijumngong and C. G. Van de Walle, "Stability, diffusivity, and vibrational properties of monatomic and molecular hydrogen in wurtzite GaN," *Phys. Rev. B* **68**, 235203 (2003).
- [87] S. S. Nekrashevich and V. A. Gritsenko, "Electronic structure of silicon dioxide (a review)," *Phys. Solid State* **56**, 207–222 (2014).
- [88] T. V. Perevalov, A. V. Shaposhnikov, K. A. Nasyrov, D. V. Gritsenko, V. A. Gritsenko, and V. M. Tapilin, "Electronic structure of ZrO₂ and HfO₂," in *Defects in High-k Gate Dielectric Stacks*, edited by Evgeni Gusev (Springer Netherlands, Dordrecht, 2006) pp. 423–434.
- [89] R. C. Vilão, A. G. Marinopoulos, H. V. Alberto, J. M. Gil, J. S. Lord, and A. Weidinger, "Sapphire α-al₂O₃ puzzle: Joint μSR and density functional theory study," *Phys. Rev. B* **103**, 125202 (2021).
- [90] P. D. C. King, T. D. Veal, P. H. Jefferson, J. Zúñiga Pérez, V. Muñoz Sanjosé, and C. F. McConville, "Unification of the electrical behavior of defects, impurities, and surface states in semiconductors: Virtual gap states in CdO," *Phys. Rev. B* **79**, 035203 (2009).
- [91] R. T. Williams, K. S. Song, W. L. Faust, and C. H. Leung, "Off-center self-trapped excitons and creation of lattice defects in alkali halide crystals," *Phys. Rev. B* **33**, 7232–7240 (1986).
- [92] K. Kan'no, T. Matumoto, and Y. Kayanuma, "Parity-broken and -unbroken self-trapped excitons in alkali halides," *Pure Appl. Chem.* **69**, 1227–1235 (1997).
- [93] B. K. Meyer, H. Alves, D. M. Hofmann, W. Kriegseis, D. Forster, F. Bertram, J. Christen, A. Hoffmann, M. Strass-

- burg, M. Dworzak, U. Haboek, and A. V. Rodina, "Bound exciton and donor-acceptor pair recombinations in ZnO," *Phys. Stat. Sol. (b)* **241**, 231–260 (2004).
- [94] B. K. Meyer, J. Sann, S. Lautenschläger, M. R. Wagner, and A. Hoffmann, "Ionized and neutral donor-bound excitons in ZnO," *Phys. Rev. B* **76**, 184120 (2007).
- [95] M. Gallart, T. Cottineau, B. Hönerlage, V. Keller, N. Keller, and P. Gilliot, "Temperature dependent photoluminescence of anatase and rutile TiO₂ single crystals: Polaron and self-trapped exciton formation," *J. Appl. Phys.* **124**, 133104 (2018).
- [96] R. Heinhold, A. Neiman, J. V. Kennedy, A. Markwitz, R. J. Reeves, and M. W. Allen, "Hydrogen-related excitons and their excited-state transitions in ZnO," *Phys. Rev. B* **95**, 054120 (2017).
- [97] X. Yang and N. C. Giles, "Hall effect analysis of bulk ZnO comparing different crystal growth techniques," *J. Appl. Phys.* **105**, 063709 (2009).
- [98] E. Yagi, R. R. Hasiguti, and M. Aono, "Electronic conduction above 4 K of slightly reduced oxygen-deficient rutile TiO_{2-x}," *Phys. Rev. B* **54**, 7945–7956 (1996).
- [99] A. Spinelli, M. A. Torija, C. Liu, C. Jan, and C. Leighton, "Electronic transport in doped SrTiO₃: Conduction mechanisms and potential applications," *Phys. Rev. B* **81**, 155110 (2010).
- [100] K. Ide, K. Nomura, H. Hosono, and T. Kamiya, "Electronic defects in amorphous oxide semiconductors: A review," *Phys. Stat. Sol. (a)* **216**, 1800372 (2019).
- [101] A. Janotti, C. Franchini, J. B. Varley, G. Kresse, and C. G. Van de Walle, "Dual behavior of excess electrons in rutile TiO₂," *Phys. Stat. Sol. RRL* **7**, 199–203.
- [102] S. Nakamura, T. Mukai, and M. Senoh, "In situ monitoring and Hall measurements of GaN grown with GaN buffer layers," *J. Appl. Phys.* **71**, 5543–5549 (1992).
- [103] D. G. Chetkine, Z. C. Feng, G. D. Gilliland, S. J. Chua, and D. Wolford, "Donor-hydrogen bound exciton in epitaxial GaN," *Phys. Rev. B* **60**, 15980–15984 (1999).
- [104] M. H. Dehn, J. K. Shenton, S. Holenstein, Q. N. Meier, D. J. Arseneau, D. L. Cortie, B. Hitti, A. C. Y. Fang, W. A. MacFarlane, R. M. L. McFadden, G. D. Morris, Z. Salman, H. Luetkens, N. A. Spaldin, M. Fechner, and R. F. Kiefl, "Observation of a charge-neutral muon-polaron complex in antiferromagnetic Cr₂O₃," *Phys. Rev. X* **10**, 011036 (2020).
- [105] M. H. Dehn, J. K. Shenton, D. J. Arseneau, W. A. MacFarlane, G. D. Morris, A. Maigné, N. A. Spaldin, and R. F. Kiefl, "Local electronic structure and dynamics of muon-polaron complexes in Fe₂O₃," *Phys. Rev. Lett.* **126**, 037202 (2021).
- [106] R. Kadono, A. Matsushita, K. Nagamine, K. Nishiyama, K. H. Chow, R. F. Kiefl, A. MacFarlane, D. Schumann, S. Fujii, and S. Tanigawa, "Charge state and diffusivity of muonium in n-type GaAs," *Phys. Rev. B* **50**, 1999–2002 (1994).
- [107] R. L. Lichti, K. H. Chow, B. Hitti, E. A. Davis, S. K. L. Sjue, and S. F. J. Cox, "Motional properties of positive muonium in gallium III-V compounds," *Physica B: Condens. Matt.* **308-310**, 862–865 (2001).
- [108] D. Gxawu, I. Z. Machi, S. H. Connell, K. Bharuth-Ram, M. J. Sithole, and S. F. J. Cox, "Diffusion of interstitial muonium, Mu_t, in a ¹³C diamond," *Diamond and Related Mater.* **14**, 375–379 (2005).
- [109] K. H. Chow, R. F. Kiefl, B. Hitti, T. L. Estle, and R. L. Lichti, "Novel behavior of bond-centered muonium in heavily doped n-type silicon: Curie-like spin susceptibility and charge screening," *Phys. Rev. Lett.* **84**, 2251–2254 (2000).
- [110] R. S. Hayano, Y. J. Uemura, J. Imazato, N. Nishida, T. Yamazaki, and R. Kubo, "Zero- and low-field spin relaxation studied by positive muons," *Phys. Rev. B* **20**, 850–859 (1979).
- [111] T. Holstein, "Studies of polaron motion: Part II. the "small" polaron," *Annals of Physics* **8**, 343–389 (1959).
- [112] See, for example, eds., Yu. M. Kagan, and A. J. Leggett, *Quantum tunneling in condensed media* (Elsevier Science Publishers, 1992).
- [113] R. F. Kiefl, R. Kadono, J. H. Brewer, G. M. Luke, H. K. Yen, M. Celio, and E. J. Ansaldo, "Quantum diffusion of muonium in KCl," *Phys. Rev. Lett.* **62**, 792–795 (1989).
- [114] R. Kadono, R. F. Kiefl, E. J. Ansaldo, J. H. Brewer, M. Celio, S. R. Kretzman, and G. M. Luke, "Delocalization of muonium in NaCl," *Phys. Rev. Lett.* **64**, 665–668 (1990).
- [115] G. M. Marshall, J. B. Warren, D. M. Garner, G. S. Clark, J. H. Brewer, and D. G. Fleming, "Production of thermal muonium in the vacuum between the grains of fine silica powders," *Phys. Lett. A* **65**, 351–353 (1978).
- [116] G. A. Beer, G. M. Marshall, G. R. Mason, A. Olin, Z. Gelbart, K. R. Kendall, T. Bowen, P. G. Halverson, A. E. Pifer, C. A. Fry, J. B. Warren, and A. R. Kunselman, "Emission of muonium into vacuum from a silica-powder layer," *Phys. Rev. Lett.* **57**, 671–674 (1986).
- [117] G. Kobayashi, Y. Hinuma, S. Matsuoka, A. Watanabe, M. Iqbal, M. Hirayama, M. Yonemura, T. Kamiyama, I. Tanaka, and R. Kanno, "Pure H⁻ conduction in oxyhydrides," *Science* **351**, 1314–1317 (2016).
- [118] K. Fukui, S. Iimura, J. Wang, T. Tada, T. Honda, K. Ikeda, T. Otomo, and H. Hosono, "Stabilization factor of anion-excess fluorite phase for fast anion conduction," *Chem. Mater.* **33**, 1867–1874 (2021).
- [119] M. J. Caldas, A. Fazzio, and A. Zunger, "A universal trend in the binding energies of deep impurities in semiconductors," *Appl. Phys. Lett.* **45**, 671–673 (1984).
- [120] W. Schmickler and J. W. Schultze, "Modern aspects of electrochemistry, vol. 17," (Plenum, New York, 1986) pp. 357–410.
- [121] P. W. Peacock and J. Robertson, "Behavior of hydrogen in high dielectric constant oxide gate insulators," *Appl. Phys. Lett.* **83**, 2025–2027 (2003).
- [122] K. Xiong, J. Robertson, and S. J. Clark, "Behavior of hydrogen in wide band gap oxides," *J. Appl. Phys.* **102**, 083710 (2007).
- [123] L. Yu, S. Lany, R. Kykyneshi, V. Jieratum, R. Ravichandran, B. Pelatt, E. Altschul, H. A. S. Platt, J. F. Wager, D. A. Keszler, and A. Zunger, "Iron chalcogenide photovoltaic absorbers," *Adv. Energy Mater.* **1**, 748–753.
- [124] A. Ennaoui, S. Fiechter, Ch. Pettenkofer, N. Alonso-Vante, K. Büker, M. Bronold, Ch. Höpfner, and H. Tributsch, "Iron disulfide for solar energy conversion," *Sol. Energy Mater. Sol. Cells* **29**, 289–370 (1993).
- [125] S. M. Wilhelm, J. Vera, and N. Hackerman, "Transport of hydrogen through pyrite," *J. Electrochem. Soc.* **130**, 2129–2132 (1983).
- [126] M. Bungs and H. Tributsch, "Electrochemical and photoelectrochemical insertion and transport of hydrogen in pyrite," *Ber. Bunsenges. Phys. Chem.* **101**, 1844–1850 (1997).
- [127] H. Okabe, M. Hiraishi, S. Takeshita, A. Koda, K. M. Kojima, and R. Kadono, "Local electronic structure of interstitial hydrogen in iron disulfide," *Phys. Rev. B* **98**, 075210 (2018).
- [128] B. Bogdanović and M. Schwickardi, "Ti-doped alkali metal aluminium hydrides as potential novel reversible hydrogen storage materials," *J. Alloys Compnd.* **253-254**, 1–9 (1997).
- [129] M. J. van Setten, V. A. Popa, G. A. de Wijs, and G. Brocks, "Electronic structure and optical properties of lightweight metal hydrides," *Phys. Rev. B* **75**, 035204 (2007).

- [130] R. Kadono, K. Shimomura, K. H. Satoh, S. Takeshita, A. Koda, K. Nishiyama, E. Akiba, R. M. Ayabe, M. Kuba, and C. M. Jensen, "Hydrogen bonding in sodium alanate: A muon spin rotation study," *Phys. Rev. Lett.* **100**, 026401 (2008).
- [131] A. Peles and C. G. Van de Walle, "Role of charged defects and impurities in kinetics of hydrogen storage materials: A first-principles study," *Phys. Rev. B* **76**, 214101 (2007).
- [132] Z. Łodziana, A. Züttel, and P. Zielinski, "Titanium and native defects in LiBH_4 and NaAlH_4 ," *J. Phys.: Condens. Matt.* **20**, 465210 (2008).
- [133] G. B. Wilson-Short, A. Janotti, K. Hoang, A. Peles, and C. G. Van de Walle, "First-principles study of the formation and migration of native defects in NaAlH_4 ," *Phys. Rev. B* **80**, 224102 (2009).
- [134] J. I. Budnick, A. Golnik, Ch. Niedermayer, E. Recknagel, M. Rossmanith, A. Weidinger, B. Chamberland, M. Filipkowski, and D. P. Yang, "Observation of magnetic ordering in La_2CuO_4 by muon spin rotation spectroscopy," *Phys. Lett. A* **124**, 103–106 (1987).
- [135] N. Nishida, H. Miyatake, D. Shimada, S. Okuma, M. Ishikawa, T. Takabatake, Y. Nakazawa, Y. Kuno, R. Keitel, J. H. Brewer, T. M. Riseman, D. L. Williams, Y. Watanabe, T. Yamazaki, K. Nishiyama, K. Nagamine, E. J. Ansaldo, and E. Torikai, "First observation of an antiferromagnetic phase in the $\text{Y}_1\text{Ba}_2\text{Cu}_3\text{O}_x$ system," *Jpn. J. Appl. Phys.* **26**, L1856–L1858 (1987).
- [136] R. H. Heffner, J. E. Sonier, D. E. MacLaughlin, G. J. Nieuwenhuys, G. M. Luke, Y. J. Uemura, William Ratcliff, S-W. Cheong, and G. Balakrishnan, "Muon spin relaxation study of $\text{La}_{1-x}\text{Ca}_x\text{MnO}_3$," *Phys. Rev. B* **63**, 094408 (2001).
- [137] G. M. Luke, L. P. Le, B. J. Sternlieb, Y. J. Uemura, J. H. Brewer, R. Kadono, R. F. Kiefl, S. R. Kreitzman, T. M. Riseman, C. E. Stronach, M. R. Davis, S. Uchida, H. Takagi, Y. Tokura, Y. Hidaka, T. Murakami, J. Gopalakrishnan, A. W. Sleight, M. A. Subramanian, E. A. Early, J. T. Markert, M. B. Maple, and C. L. Seaman, "Magnetic order and electronic phase diagrams of electron-doped copper oxide materials," *Phys. Rev. B* **42**, 7981–7988 (1990).
- [138] S. Yunoki, A. Moreo, E. Dagotto, S. Okamoto, S. S. Kancharla, and A. Fujimori, "Electron doping of cuprates via interfaces with manganites," *Phys. Rev. B* **76**, 064532 (2007).